
Toward Unlimited Self-Learning Monte Carlo with Annealing Process Using VAE’s Implicit Isometricity

Yuma Ichikawa
Fujitsu Limited

Akira Nakagawa
Fujitsu Limited

Hiromoto Masayuki
Fujitsu Limited

Yuhei Umeda
Fujitsu Limited

Abstract

Self-learning Monte Carlo (SLMC) methods are recently proposed to accelerate Markov chain Monte Carlo (MCMC) methods by using a machine learning model. With generative models having latent variables, SLMC methods realize efficient Monte Carlo updates with less autocorrelation. However, SLMC methods are difficult to directly apply to multimodal distributions for which training data are difficult to obtain. In this paper, we propose a novel SLMC method called the “annealing VAE-SLMC” to drastically expand the range of applications. Our VAE-SLMC utilizes a variational autoencoder (VAE) as a generative model to make efficient parallel proposals independent of any previous state by applying the theoretically derived implicit isometricity of the VAE. We combine an adaptive annealing process to the VAE-SLMC, making our method applicable to the cases where obtaining unbiased training data is difficult in practical sense due to slow mixing. We also propose a parallel annealing process and an exchange process between chains to make the annealing operation more precise and efficient. Experiments validate that our method can proficiently obtain unbiased samples from multiple multimodal toy distributions and practical multimodal posterior distributions, which is difficult to achieve with the existing SLMC methods.

et al., 2013). Markov chain Monte Carlo (MCMC) methods are powerful and versatile numerical methods for sampling from such probability distributions. MCMC methods generate a sequence of samples that converge to the target distribution. The transition probability is determined on the basis of detailed balance conditions. As a practical example, the accept/reject process of Metropolis–Hastings (Hastings, 1970) can guarantee the detailed balance condition for any proposal distribution satisfying the mild condition. Although theoretical guarantees exist, convergence and mixing depend on a proposal distribution.

Among recent advances in machine learning, a general method called the self-learning Monte Carlo (SLMC) method (Liu et al., 2017) was introduced to accelerate MCMC simulations by training a machine learning model to propose uncorrelated states in the Markov chain and has been applied to various problems (Xu et al., 2017; Shen et al., 2018). In particular, a generative model with latent variables realize efficient global update through the obtained information-rich latent representation (Huang and Wang, 2017; Albergo et al., 2019; Monroe and Shen, 2022; Tanaka and Tomiya, 2017). Although powerful, the performance of SLMC simulation strongly depends on the properties of the machine learning model and the quality of training data to train the machine learning model. For example, it is challenging to directly use SLMC for multimodal distributions because obtaining unbiased training data among all modes is difficult.

In this paper, we propose a novel SLMC method called “annealing VAE-SLMC” to substantially expand the scope of application of the SLMC method in various fields. Specifically, we introduce a variational autoencoder (VAE) to the SLMC method as a generative model by applying the theoretically derived closed-form likelihood from the implicit isometric property of VAE (Nakagawa et al., 2021). This makes efficient parallel proposals between modes independent of any previous state. We also propose an adaptive annealing process, like a simulated annealing process (Kirkpatrick et al., 1983), and make the method applicable to the cases where obtaining unbiased training data is difficult. Furthermore, we combine a parallel annealing process and an exchange process between Markov chains, like

1 INTRODUCTION

High-dimensional probability distributions for which the normalizing factor is not analyzable appear in a wide variety of fields. For example, they appear in condensed-matter physics (Binder et al., 1993; Baumgärtner et al., 2012), biochemistry (Manly, 2018), and Bayesian inference (Martin et al., 2011; Gelman et al., 1995; Foreman-Mackey

the exchange Monte Carlo method (Swendsen and Wang, 1986; Hukushima and Nemoto, 1996), making the annealing VAE-SLMC more efficient and precise. Our contributions are summarized as follows:

- The VAE-SLMC is proposed to improve the efficiency of parallel proposals with an SLMC method, by using theoretically derived implicit isometricity of the VAE.
- An adaptive annealing process is proposed to expand the applicability of the VAE-SLMC to the cases where obtaining unbiased training data is difficult.
- For further efficiency, a parallelization method that combines the parallel annealing process and an inter-chain exchange process is proposed.
- Through numerical experiments, we demonstrate that our method is applicable to various difficult problems such as multimodal toy distribution, multimodal posterior, and optimization problems with multiple globally optimal solutions.

2 BACKGROUND

2.1 Metropolis–Hastings Algorithm

We start this section by illustrating the Metropolis–Hastings method (Hastings, 1970). We define p as a target distribution on a state space \mathcal{X} where the normalizing factor is not necessarily tractable. Then we introduce $\tilde{p} \propto p$, which can be expressed as a closed form. To obtain samples from p , we use an MCMC method to construct a Markov chain whose stationary distribution is p . The objective of the MCMC method is to obtain a sequence of correlated samples from the target distribution p , where the sequence can be used to compute an integral such as an expected value.

The Metropolis–Hastings algorithm is a generic method to construct the Markov chain (Hastings, 1970). The Metropolis–Hastings algorithm prepares a conditional distribution q called a proposal distribution, which satisfies irreducibility, and the Markov chain $(x^{(t)})_{t=0}^T$ proceeds via the following steps: starting from $x^{(0)} \sim \pi_0$, where $\pi^{(0)}$ is the initial distribution, at each step t , proposing $x' \sim q(x' | x^{(t)})$, and with probability

$$A(x' | x^{(t)}) = \min \left(1, \frac{\tilde{p}(x')q(x^{(t)} | x')}{\tilde{p}(x_t)q(x' | x^{(t)})} \right),$$

accept x' as the next update $x^{(t+1)} = x'$ or with probability $1 - A(x' | x^{(t)})$, reject x' and retain the previous state $x^{(t+1)} = x^{(t)}$. The proposal distribution $q(x' | x^{(t)})$ is prepared for typically a local proposal, such as $q(x' | x^{(t)}) = \mathcal{N}(x' | x^{(t)}, \Sigma)$, where a scale parameter Σ for the continuous probability distribution. Hereafter, such a method

is referred to as a local update MCMC method. Note that the calculation of the acceptance probability only requires the ratio of probability distributions (i.e., calculation of the normalizing factor is not required).

Although the local update MCMC methods have a theoretical asymptotic guarantee for almost arbitrary proposal distributions, in practice, the performance of the algorithm depends on the choice of the proposal distribution q .

2.2 Self-learning Monte Carlo

Motivated by the developments of machine learning, a general method, known as the self-learning Monte Carlo (SLMC) method, has been proposed. In this method, the information of samples generated by a local update MCMC method is extracted by a machine learning model $p_\theta(x)$ and the MCMC simulation is accelerated with the model $p_\theta(x)$. Specifically, the SLMC method sets the proposal distribution as $q(x' | x^{(t)}) = p_\theta(x')$ and the acceptance probability is expressed as

$$A(x' | x^{(t)}) = \min \left(1, \frac{\tilde{p}(x')p_\theta(x^{(t)})}{\tilde{p}(x^{(t)})p_\theta(x')} \right). \quad (1)$$

If we obtain a perfect machine learning model such that $p = p_\theta$, the acceptance probability is 1. Moreover, if the proposal $x' \sim p_\theta(x')$ is accepted, the state will be uncorrelated with the any previous state because the proposal probability $p_\theta(x')$ is independent of the previous state $x^{(t)}$.

Note that the machine learning model $p_\theta(x)$ for the SLMC method is desired to have the following three properties:

1. The model should have the expressive power to well approximate the target probability distribution $p(x)$.
2. Both proposals and acceptance probabilities in Eq. (1) should be computed from the machine learning model $p_\theta(x)$ at low cost.
3. Unbiased training data should be available to train the machine learning model $p_\theta(x)$.

If the first property is unsatisfied, the proposed state x' is rarely accepted and the correlation between samples becomes large. If the second property is unsatisfied, then, even if a good machine learning model $p_\theta \approx p$ is obtained, the SLMC simulation will not be efficient because of the cost of proposing a new state x' and computing the acceptance probability in Eq. (1). If the third property is not satisfied, the SLMC method will generate biased samples in practical sense due to slow mixing, etc. because the model can hardly propose a state that is not included in the training data.

2.3 Implicit Isometricity of the VAE

A VAE (Kingma and Welling, 2013) is a generative model with latent variables, and its purpose is to model the probability distribution behind the data. Let $\mathcal{D} = \{x^\mu\}_{\mu=1}^P$, $x^\mu \in \mathbb{R}^D$ be training data and $p_{\mathcal{D}}(x)$ be the empirical distribution of the training data. Specifically, the VAE is a probability model of the form $p_\theta(x, z) = p_\theta(x | z)p_\theta(z)$, where $z \in \mathbb{R}^M$ is the latent variable with prior $p_\theta(z)$, which is a standard normal distribution widely used as a prior. The VAE is trained by maximizing the following evidence lower bound (ELBO) of log-likelihood with variational posterior $q_\phi(z | x) = \mathcal{N}(z; \mu_\phi(x), \sigma_\phi(x))$, where $\mu_\phi(x) = (\mu_{m,\phi}(x))_{m=1}^M$, $\sigma_\phi(x) = (\sigma_{m,\phi}(x))_{m=1}^M$ is an estimating parameter, since direct maximization of the log-likelihood is difficult:

$$\begin{aligned} \mathbb{E}_{p_{\mathcal{D}}} [\mathbb{E}_{q_\phi} [\log p_\theta(x | z)] - D_{\text{KL}}[q_\phi(z | x) \| p(z)]] \\ \equiv \mathbb{E}_{p_{\mathcal{D}}} [\mathcal{L}_{\text{ELBO}}(x, \theta, \phi)], \end{aligned} \quad (2)$$

where $D_{\text{KL}}[\cdot \| \cdot]$ and $\mathcal{L}_{\text{ELBO}}$ denote Kullback–Leibler divergence and ELBO, respectively. $p_\theta(x | z)$ and $q_\phi(z | x)$ are called a decoder and an encoder, respectively, and the first term in Eq. (2) is called a reconstruction loss. In β -VAE (Higgins et al., 2016), $\beta_{\text{VAE}} \in \mathbb{R}_+$ is introduced to control the trade-off between the first and second terms of Eq. (2). Thus the objective function of the β -VAE becomes

$$\begin{aligned} \mathbb{E}_{p_{\mathcal{D}}} [\mathbb{E}_{q_\phi} [\log p_\theta(x | z)] - \beta_{\text{VAE}} D_{\text{KL}}[q_\phi(z | x) \| p(z)]] \\ \equiv \mathbb{E}_{p_{\mathcal{D}}} [\mathcal{L}(x, \theta, \phi; \beta_{\text{VAE}})]. \end{aligned} \quad (3)$$

Recently, extensive work has been done to clarify the theoretical properties of VAEs. Rolinek et al. (2019) have theoretically shown that the Jacobian matrix of a VAE is orthogonal. Nakagawa et al. (2021) have theoretically shown and numerically verified that a β -VAE performs implicit isometric embedding to the latent space with an appropriate scaling under mild conditions. In the isometric embedding, the distances and the probabilities in the input space are preserved in the latent space (Han and Hong, 2006). From the results, if the reconstruction loss is the sum of squared errors (SSE) and the prior $p_\theta(z)$ is a standard normal distribution, then the following holds:

$$p_\theta(x) \propto \mathcal{N}(\mu_\phi(x); 0_M, I_M) \prod_{m=1}^M \sigma_{m,\phi}(x) \equiv \Gamma_\theta(x), \quad (4)$$

where $0_M = (0, \dots, 0) \in \mathbb{R}^M$ and I_M denotes an M -dimensional identity matrix. For the detailed proof and consistency through numerical experiments, refer to Nakagawa et al. (2021); see Supplementary Material B.1 for the evaluation of implicit isometricity. Note that the reconstruction loss can be extended to the cases rather than SSE (Nakagawa et al., 2021).

3 ANNEALING SELF-LEARNING MONTE CARLO WITH VAE

To satisfy the desired properties of the SLMC method in Sec. 2.2, we first propose a novel SLMC method with a VAE called “VAE-SLMC,” and then propose an annealing process for it. In addition, we also propose two extensions, adaptive scheduling and parallel exchanging.

3.1 Self-learning Monte Carlo with VAE

Our VAE-SLMC method adopts a VAE as a machine learning model $p_\theta(x)$ and takes advantage of the VAE’s implicit isometricity to calculate acceptance probability efficiently. We can easily compute $\Gamma_\theta \propto p_\theta$ from Eq. (4) by passing the state x through the encoder $q_\phi(z | x)$, and the acceptance probability of the VAE-SLMC becomes

$$A(x' | x^{(t)}) = \min \left(1, \frac{\tilde{p}(x') \Gamma_\theta(x^{(t)})}{\tilde{p}(x^{(t)}) \Gamma_\theta(x')} \right). \quad (5)$$

Here, the normalizing factor of Eq. (4) is unnecessary because the acceptance probability only includes the probability ratio. The VAE can generate samples $x' \sim p_\theta(x)$ at a low cost through the following procedure: The VAE first generates the latent variables, $z \sim \mathcal{N}(z; 0_M, I_M)$ and then generates samples by passing the latent variables z through the decoder $p_\theta(x | z)$. A well-trained VAE can make parallel proposals between modes independent of any previous state due to information-rich latent space.

A detailed flow of the VAE-SLMC is shown in Algorithm 1. The model is iteratively updated by the “retrain step,” where the model is retrained with the samples generated by itself. Note that VAE-SLMC is applicable to discrete probability distributions.

3.2 Annealing Process for Bias-free Training Data

A successful SLMC simulation strongly depends on the quality of training data to train the machine learning model $p_\theta(x)$. Especially in the case of multimodal probability distribution, it is difficult to obtain training samples covering all the modes in the target distribution. To solve this problem, we propose an annealing VAE-SLMC, in which an annealing process like simulated annealing (Kirkpatrick et al., 1983) is added to the VAE-SLMC. First, we introduce inverse temperature β for a range of values $0 \leq \beta \leq 1$ to a target distribution p and $\tilde{p} \propto p$ as

$$p(x; \beta) = \frac{p(x)^\beta}{\int p(x)^\beta dx}, \quad \tilde{p}(x; \beta) = \tilde{p}(x)^\beta, \quad (6)$$

and then increase β from a small value (i.e., high temperature) to 1 like simulated annealing. Note that $p(x; \beta = 1) = p(x)$, and $p(x; \beta = 0)$ is a uniform distribution over the state space of the random variable. Typically, smaller

Algorithm 1 VAE-SLMC

```

1: function VAE-SLMC( $\tilde{p}(x)$ ,  $p_\theta(x)$ ,  $\Gamma_\theta(x)$ ;  $T$ ,  $T_{\text{train}}$ ,
    $\mathcal{D}, \pi_0$ )
2:   Initialize  $x^{(0)} \sim \pi_0$ 
3:   while  $t \leq T$  do
4:     Generate  $x' \sim p_\theta(x)$ 
5:     Calculate  $A(x' | x^{(t)})$  by Eq. (5)
6:     if  $(A(x' | x^{(t)}) > U[0, 1])$  then
7:        $x^{(t+1)} \leftarrow x'$ 
8:     else
9:        $x^{(t+1)} \leftarrow x^{(t)}$ 
10:    end if
11:    if  $t \equiv 0 \pmod{T_{\text{train}}}$  then  $\triangleright$  Retrain Step
12:      Make training data  $\mathcal{D}^{(t)}$  from  $(x^{(t)})_{t=0}^t$   $\triangleright$ 
      use nearly independent sequence of samples
13:      Set  $\mathcal{D} \leftarrow \mathcal{D} \cup \mathcal{D}^{(t)}$ 
14:      Train  $p_\theta(x)$  with  $\mathcal{D}$  and update  $\Gamma_\theta(x)$ 
15:    end if
16:     $t \leftarrow t + 1$ 
17:  end while
18:  return samples  $(x^{(t)})_{t=0}^T$ 
19: end function

```

β allows easier exploration for multiple modes in the complex distribution.

The detailed flow of the annealing VAE-SLMC is shown in Algorithm 2 and abstracted in Fig. 1. First, we set up a β sequence $\{\beta_k\}_{k=0}^K$, $\beta_0 \leq \dots \leq \beta_K = 1$, where β_0 is set sufficiently small for the local update MCMC method to efficiently explore. Second, we acquire the training data from the $p(x; \beta_0)$ by the local update MCMC method and train the model $p_{\theta_0}(x; \beta_0)$ with the training data. Third, we acquire the training data again from the $p(x; \beta_1)$ by the VAE-SLMC with the model $p_{\theta_0}(x; \beta_0)$ and then train the model $p_{\theta_1}(x; \beta_1)$ with the training data from $p(x; \beta_1)$. We set the initial parameters of training the model $p_{\theta_1}(x; \beta_1)$ as θ_0 since $p_{\theta_0}(x; \beta_0)$ and $p_{\theta_1}(x; \beta_1)$ are expected to have a similar common structure when $\beta_1 \approx \beta_0$, leading to a similar effect like pre-training. By repeating this process until $\beta_K = 1$, finally we obtain accurate samples from the $p(x; \beta_K = 1)$. In general, rather than VAEs, this process can also be applied to other models that easily propose all modes of the target distribution to avoid losing information during the learning process and satisfy the desired conditions explained in Sec. 2.2.

3.3 Adaptive β Scheduling for Annealing Process

The annealing process is sensitive to how the β sequence is determined. Simply setting an arithmetic progression β sequence $\{\beta_0 + k\Delta\beta\}_{k=0}^{K-1}$ often requires extra computation time and results in biased samples in practical sense because of a lack of model learning; see Supplementary Material D.1 for the failure behavior. Thus, we propose

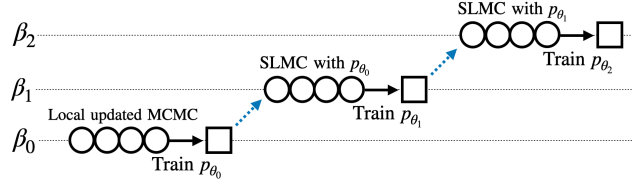


Figure 1: A graphical model of the annealing process. A circle denotes a state of a Markov chain with the stationary distribution $p(x; \beta_k)$ and a square represents a state of the model. A black solid arrow means training of the model and a blue dashed arrow expresses the annealing procedure.

a method to adaptively determine the β sequence, following the two β -search strategies shown in Fig. 2. Note that these two strategies can be used together as the algorithm in Supplementary Material C.2.

Parallel search. The candidates of $\{\beta'_{(s)}\}_{s=0}^S$ are generated in parallel to determine β_{k+1} from β_k . The acceptance rates $\{\text{AR}(\beta'_{(s)})\}_{s=1}^S$ with respect to $\{p(x; \beta'_{(s)})\}_{s=0}^S$ are then estimated in parallel by a typically small VAE-SLMC simulation with the model $p_{\theta_k}(x; \beta_k)$, taking advantage of the fact that a VAE can make parallel proposals completely independent of any previous states. After that, the $\beta'_{(s)}$ that satisfies $\text{AR}_{\min} \leq \text{AR}(\beta'_{(s)}) \leq \text{AR}_{\max}$ is selected as a candidate of β_{k+1} . Note that AR_{\min} and AR_{\max} are lower and upper bounds determined by a user. If there exist multiple candidates, a single candidate is selected according to user-defined criteria (e.g., the smallest $\beta'_{(s)}$ is selected).

Sequential search. First, a candidate $\beta'_{(0)} \geq \beta_k$ is generated and the acceptance rate $\text{AR}(\beta'_{(0)})$ with respect to $p(x; \beta'_{(0)})$ is calculated by a typically small SLMC simulation with the model $p_{\theta_k}(x; \beta_k)$. Then, if $\text{AR}(\beta'_{(0)})$ is between AR_{\min} and AR_{\max} , the candidate $\beta'_{(0)}$ is accepted as β_{k+1} , otherwise, it is rejected and another candidate $\beta'_{(1)}$ is generated by

$$\beta'_{(1)} \leftarrow \begin{cases} \beta'_{(0)} + \varepsilon & (\text{AR}(\beta'_{(0)}) \geq \text{AR}_{\max}) \\ \beta'_{(0)} - \varepsilon & (\text{AR}(\beta'_{(0)}) \leq \text{AR}_{\min}) \end{cases},$$

where ε is a positive constant determined by a user. The new candidate $\beta'_{(1)}$ is checked whether it is accepted or not in the same way as described above. This process is repeated until the s -th candidate $\beta'_{(s)}$ is accepted, and finally $\beta'_{(s)}$ is set to β_{k+1} .

It should be noted that the proposed method has an implicit function to detect insufficient learning of the model $p_{\theta_k}(x; \beta_k)$ and retrain it. If the model is not trained enough, the candidates $\beta'_{(s)}$ are all rejected and $\beta_{k+1} = \beta'_{(s)}$ remains equal to β_k . From Algorithm 1, such a behavior induces retraining of the model with the same β_k . This

Algorithm 2 Annealing VAE-SLMC

Input target distribution $\tilde{p}(x; \beta)$, initial model $p_{\theta_0}(x; \beta_0)$, β -sequence $\{\beta_k\}_{k=0}^K$, initial distribution π_0 , training data \mathcal{D} .

- 1: Initialize $x^{(0)} \sim \pi_0$
- 2: **for** $k = 1$ to K **do**
- 3: Set $(x_k^{(t)})_{t=0}^T = \text{VAE-SLMC}(\tilde{p}(x; \beta_k), p_{\theta_{k-1}}(x; \beta_{k-1}), \Gamma_{\theta_{k-1}}(x; \beta_{k-1}); T, T_{\text{train}}, \pi_0, \mathcal{D}_{k-1})$ from Algorithm 1.
- 4: Make the training data \mathcal{D}_k from $(x_k^{(t)})_{t=0}^T$
- 5: Train p_{θ_k} with \mathcal{D}_k
- 6: **end for**
- 7: Set $(x_K^{(t)})_{t=0}^T = \text{VAE-SLMC}(\tilde{p}(x; \beta_K), p_{\theta_K}(x; \beta_K), \Gamma_{\theta_K}(x; \beta_K); T, T_{\text{train}}, \pi_0, \mathcal{D}_K)$

Output samples $(x_K^{(t)})_{t=0}^T$

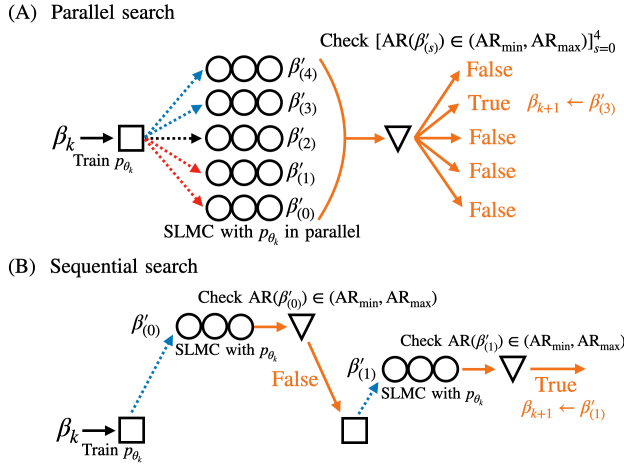


Figure 2: Graphical models illustrating the adaptive annealing process. A triangle is a checking process for an acceptance rate, and the other notations are same as in Fig. 1. If the check is True, output next β_{k+1} .

is a great advantage of the proposed method over simple scheduling such as logarithmic scheduling.

3.4 Parallel Annealing Exchange SLMC Method

Although the adaptive β scheduling methods are effective, they cannot deal with the cases where the training data fail to cover some part of the target distribution. If the adaptive annealing VAE-SLMC includes the model $p_{\theta_k}(x; \beta_k)$ that trains only part of the target distribution, it generates biased samples at steps larger than β_k . To mitigate this problem, we propose another method to improve the annealing process of the VAE-SLMC, called parallel annealing exchange SLMC (ESLMC). The ESLMC combines a parallel annealing process and an exchange process used by a replica exchange Monte Carlo (EMC) method (Swendsen and Wang, 1986; Hukushima and Nemoto, 1996).

We first set up a sequence of inverse temperature $\{\beta_0^j\}_{j=0}^J$, $\beta_0^0 \geq \dots \geq \beta_0^J$ where the upper/lower index represents the parallel chain/annealing step. Second, we acquire the

training data from $\{p(x^j; \beta_0^j)\}_{j=1}^J$ with a local update EMC method and train the models $\{p_{\theta_0^j}(x; \beta_0^j)\}_{j=0}^J$ with the training data. As with the annealing VAE-SLMC, the training starts from β_0^0 to β_0^J , where the parameters of the previous model are used as initial values to train the next model, expecting to a pre-training effect. We then acquire the training data from $\{p(x^j; \beta_1^j)\}_{j=1}^J$ by the SLMC method with the models $\{p_{\theta_0^j}(x; \beta_0^j)\}_{j=0}^J$ including exchange process of following acceptance probability,

$$A(x^j, x^{j+1}) = \min \left(1, \frac{\tilde{p}(x^{j+1}; \beta_0^j) \tilde{p}(x^j; \beta_0^{j+1})}{\tilde{p}(x^j; \beta_0^j) \tilde{p}(x^{j+1}; \beta_0^{j+1})} \right), \quad (7)$$

and then again train the models $\{p_{\theta_1^j}(x; \beta_1^j)\}_{j=0}^J$ with the training data. We can obtain accurate samples from the target distribution by repeating the process until $\beta_K^J = 1$. Note that the sequence $\{\beta_k^j\}_{j=1}^J$ is set so that the inverse temperatures are well exchanged between chains under the acceptance probability of Eq. (7). Even with this swap, the steady state of the Markov chain for each inverse temperature $\{\beta_k^j\}_{j=1}^J$ is guaranteed to be $\{p(x^j; \beta_k^j)\}_{j=1}^J$ for each of them. This exchange can be considered automatic annealing by random walking in the inverse temperature direction. That is, fast mixing occurs in β_k^0 , which is relatively easy to explore, and its effect positively affects the mixing of MCMC with large inverse temperatures.

Even if the model $p_{\theta_k^j}(x_k^j; \beta_k^j)$ fails to learn complete information of the target distribution, the inter-chain exchange process makes the training data for the model $p_{\theta_{k+1}^j}(x_{k+1}^j; \beta_{k+1}^j)$ the bias-less samples (i.e., by the inter-chain exchange process, chains that almost completely learn the target distribution can help other chains that fail to learn). In addition, with the larger number of parallel chains, the fewer times annealing will be performed up to $\beta_K^J = 1$. We can also apply the adaptive annealing process in Sec. 3.3 to the ESLMC; see Supplementary Material C.2 for detailed implementation.

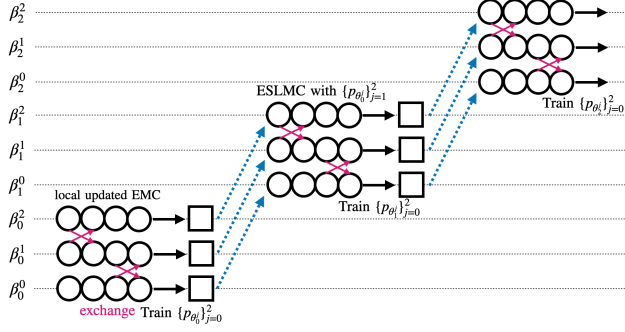


Figure 3: A graphical model illustrating the parallel annealing ESLMC method. Pink crossed arrows denote a exchange process between chains, and the other notations are same as in Fig. 1.

Table 1: Experimental Conditions and Abbreviations

Method (Section)	Anneal. (3.2)	Adapt. (3.3)	Parallel (3.4)	Proposal
CA-VAE-SLMC	✓			VAE
AA-VAE-SLMC	✓	✓		VAE
CA-VAE-ESLMC	✓		✓	VAE
AA-VAE-ESLMC	✓	✓	✓	VAE
HMC-EMC			✓	HD
MH-EMC			✓	RW
MH				RW

4 NUMERICAL EXPERIMENT

We validate the performance of the proposed method on multi-cluster Gaussian mixture distributions, real-world application to a Bayesian inference of multimodal posterior for spectral analysis, and an optimization problem with multiple global optima.

Table 1 summarizes the experimental conditions and their abbreviations. RW and HD in the proposal column of the table denote random walk proposal $\mathcal{N}(x' | x^{(t)}, \sigma^2 I_D)$ where σ is scale factor and Hamilton dynamics (Duane et al., 1987), respectively. We experimented with four combinations of our proposed methods.

The parameters of MH, MH-EMC, and HMC-EMC are well tuned. We provide details of instances, implementations, and metrics in Supplementary Material E.

4.1 Gaussian Mixture

We generalized the two Gaussian mixture proposed in (Woodard et al., 2009) to multi-Gaussian mixture. Specifically, each cluster $C = [1, 2, 3, 4, 5]$ is assumed to be Gaussian with variance $\sigma^2 = 0.5\sqrt{D}/100$ in the $D = [2, 10, 25, 50, 100]$ dimension, the distance between each cluster is assumed to be equal, and the overall mean is as-

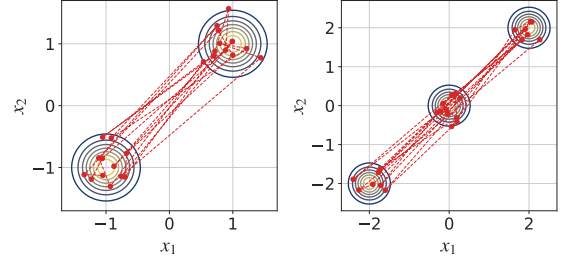


Figure 4: The transition of the AA-VAE-SLMC method on a two- or three Gaussian mixture. The contour lines represent the target distribution, the red dots are the sample sequence generated by the AA-VAE-SLMC, and the dotted lines represent the first 25 transitions.

sumed to be 0. Performance is measured via the root mean squared error (RMSE) defined as the Euclidian distance between the true expected value and its empirical estimate.

Initial learning. For the CA-VAE-SLMC and AA-VAE-SLMC, we first train the VAE with 40,000 training data at $\beta_0 = 0.1$, which are generated using a local update MC method. For the CA-VAE-ESLMC and AA-VAE-ESLMC, we first train the VAEs with 40,000 training data generated by the MH-EMC on two chains with $\{\beta_0^0 = 0.1, \beta_0^1 = 0.25\}$, where $\beta_0^1 = 0.25$ is tuned so that the exchange acceptance rate becomes approximately in a range of 0.2–0.3.

Annealing process. The CA-VAE-SLMC uses a β sequence having 20 values with uniform intervals from $\beta_0 = 0.1$ to 1.0. The AA-VAE-SLMC is based on setting AR_{\min} to 0.2 and AR_{\max} to 1.0. The CA-VAE-ESLMC uses two parallel chains starting with $\{\beta_0^0, \beta_0^1\}$. The first chain uses 10 equally spaced β sequences from β_0^0 to $1.0 - (\beta_0^1 - \beta_0^0)$ and the second chain also uses 10 equally spaced β sequences from β_0^1 to 1.0 for comparison with the CA-VAE-SLMC, which has the same computational cost except for the exchange process between chains with one thread. The AA-VAE-ESLMC also uses two parallel chains starting with $\{\beta_0^0, \beta_0^1\}$ and set AR_{\min} to 0.2 and AR_{\max} to 1.0 for the two chains.

Results of adaptive annealing VAE-SLMC. Figure 4 shows the dynamic transitions between the modes by AA-VAE-SLMC for a two- or three-cluster 2D Gaussian mixture. Due to the information-rich latent space of the VAE, the proposed method successfully realizes almost equally transitions between clusters at the early stage of the simulation, which is not possible for the local update MCMC method. Figure 5 shows the results when either K or D is varied and the other is fixed ($D = 10$ or $K = 3$). The RMSEs drastically decrease under all circumstances, compared with MH and HMC-EMC for the simplest case.

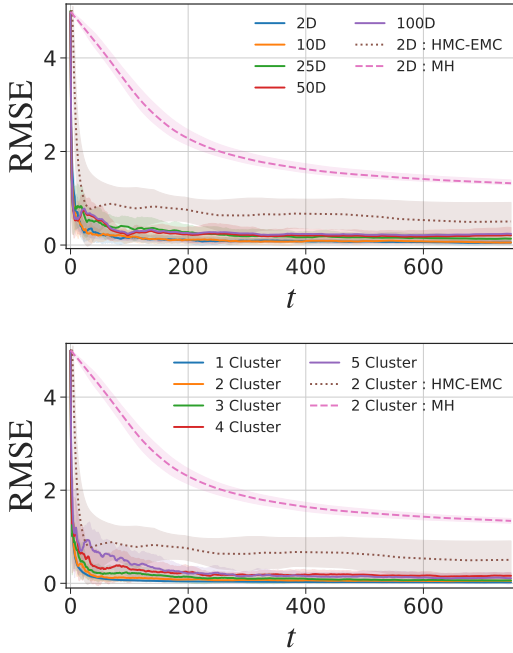


Figure 5: AA-VAE-SLMC method in Gaussian mixture. Every solid line/shaded area depicts the mean/standard deviation of RMSE averaged across 10 independent chains after t -th Monte Carlo step. (Top) RMSE for Gaussian mixtures with fixed cluster $C = 3$ and varying dimension D . (Bottom) RMSE for Gaussian mixtures with a fixed $D = 10$ and varying cluster M .

Ablation study. We thoroughly compare the four methods listed in Table 1 on five-cluster 10D Gaussian mixture. Figure 6 shows the RMSEs, β transition after k -th annealing, and the acceptance rate for each method. The RMSEs for all the proposed methods in Table 1 show almost same behaviors and decrease more rapidly than HMC-EMC and MH. The AA-VAE-ESLMC had the lowest number of the annealing process, as expected. In addition, although the property of the distribution itself is also relevant, effects such as the pre-learning, described in the Sec. 3, appear to increase the acceptance rates of CA-VAE-SLMC and CA-VAE-ESLMC and the annealing intervals of AA-VAE-SLMC and AA-VAE-ESLMC, which implies that we can significantly reduce the learning steps at each annealing, leading to tremendous speedups.

4.2 Spectral Analysis

Motivated by (Luengo et al., 2020), we demonstrate real-world Bayesian estimation of a noisy multi-sinusoidal signal; see Supplementary Material D.4 for the additional experiment of real-world Bayesian estimation of sensor net-

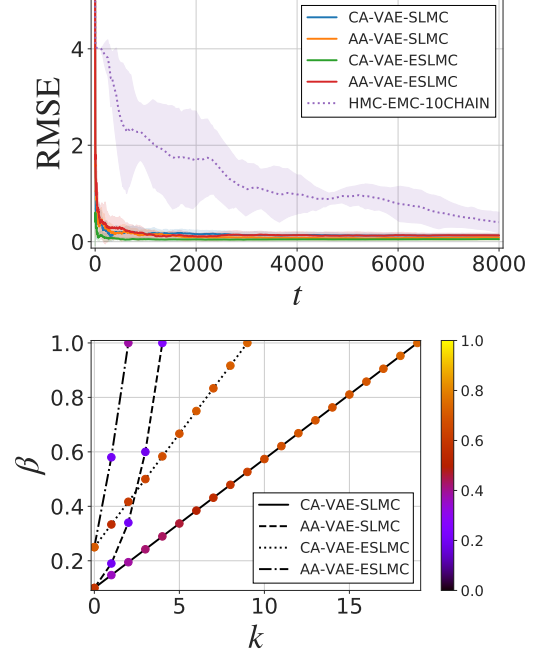


Figure 6: Comparison of methods in Table 1. (Top) Every solid line/shaded area depicts the mean/standard deviation of RMSE averaged across 10 independent chains after t -th Monte Carlo step. (Bottom) β transition after k -th annealing. The color bar denotes the acceptance rates, and acceptance rates steps.

work localization problems. The signal is given by

$$y(\tau) = A_0 + \sum_{d=1}^D A_d \cos(2\pi f_d \tau + \phi_d) + r(\tau), \quad \tau \in \mathbb{R},$$

where A_0 is a constant term, $A \equiv \{A_d\}_{d=1}^D$ is a set of amplitudes, $f \equiv \{f_d\}_{d=1}^D$ are frequencies, $\phi \equiv \{\phi_d\}_{d=1}^D$ are their phases, and $r(\tau)$ is an additive white Gaussian noise. The estimation of the parameters is important in a variety of applications, such as signal processing (Stoica, 1993; So et al., 2005), control engineering (Bodson and Douglas, 1997; Bobtsov and Pyrkin, 2012). Here we compute the posterior for frequencies $f \in \mathbb{R}^8$ given the data by discretizing $y(\tau)$. Note that the problem is symmetric with respect to hyperplane $f_1 = \dots = f_D$ and the marginal posterior is multimodal (see Fig. 7). Performance is measured via the relative error of the estimated mean (REM) in all dimensions. We apply AA-VAE-SLMC starting from $\beta_0 = 0.1$, setting $\text{AR}_{\min} = 0.15$ and $\text{AR}_{\max} = 1.0$. Figure 7 shows the REM is rapidly decreased compared with MH-EMC and all modes are covered in the first few transitions.

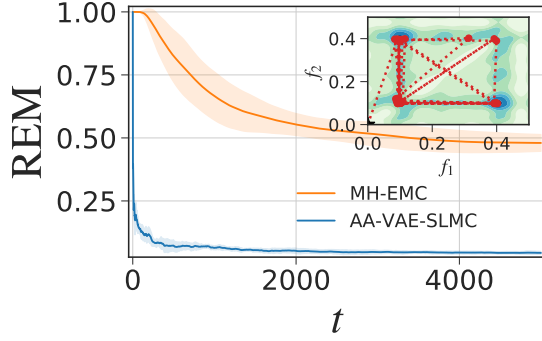


Figure 7: The relative error of the estimated mean (REM) for spectral analysis after t -th Monte Carlo step. Every solid line/shaded area depicts the mean/standard deviation of REM averaged across 10 independent chains. In the inset figure, the contour line represents the marginal posterior, and the red dotted line represents the first 30 transitions.

4.3 Optimization Problem

By considering the cost function to minimize as a negative log-likelihood and annealing to sufficiently large β , the optimization problem can be solved in the same way as simulated annealing (Kirkpatrick et al., 1983). Here, we demonstrate our method is extremely effective in searching for multiple globally optimal solutions. Specifically, we confirm the behavior of AA-VAE-SLMC on the following Himmelblau function (Himmelblau et al., 2018):

$$f(x_1, x_2) = -(x_1^2 + x_2 - 11)^2 - (x_1 + x_2^2 - 7)^2. \quad (8)$$

It is one of the famous optimization problems with the following 4 global optima:

$$(x_1^*, x_2^*) = (3.0, 2.0), (-2.805118, 3.131312), \\ (-3.779310, -3.283186), (3.584428, -1.848126).$$

See Supplementary Material D.5 for additional results of application to other high-dimensional functions with multiple local optimal. We use AA-VAE-SLMC method starting from $\beta_0 = 0.1$ to $\beta_k = 50$ and set $\text{AR}_{\min} = 0.25$ and $\text{AR}_{\max} = 1.0$;

Figure 8 shows that the generated samples consist only of states near the optimal solution and that the four optimal values are generated with almost equal probability, whose global transition is effective complex optimization problems. The acceptance rate is about 0.43, and the RMSE between the estimated value of the function and the true optimal value of the function is $1.18 \times 10^{-3} \pm 4.0 \times 10^{-4}$ across 10 chain average and standard deviation up to 50,000 iterations.

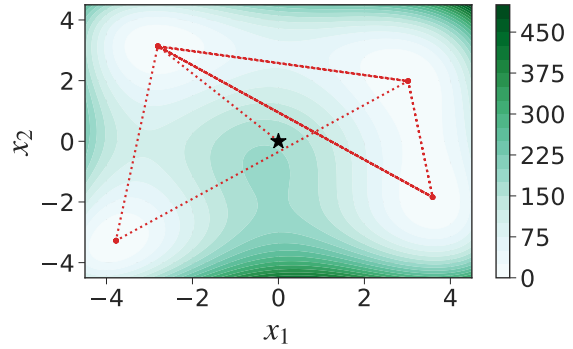


Figure 8: Snapshot of the global optimal solution search with AA-VAE-SLMC at $\beta_K = 50$. The red dotted line represents the first 30 transitions. The star point is the initial value, from which four transitions to the global optimum are made with almost equal probability.

5 RELATED WORK

SLMC methods with generative model with latent variables have been proposed. They do not provide specific algorithms for situations where obtaining training data are challenging. First, an SLMC with the restricted Boltzmann machine (RBM) (Huang and Wang, 2017) has been proposed, and the RBM resulted in an efficient global transition. The proposal of the RBM requires the MCMC simulation to be implemented by parallel alternating Gibbs sampling of hidden and visible variables. However, this method can cause problems related to long correlation times (Roussel et al., 2021). An SLMC with a flow-based model has also been considered (Albergo et al., 2019). The SLMC does not require MCMC and needs to worry about mixing. However, the flow-based model requires strong restrictions for the networks. Similar to our method is the SLMC with a VAE proposed by (Monroe and Shen, 2022). This method does not require MCMC and has no restriction on the network; however, this method is based on an approximation $p_\theta(z | x) \approx q_\phi(z | x)$, whose approximation can lead to a significant decrease in the acceptance rate. Moreover, evaluating the validity of the approximation at a low cost is difficult. Our proposed method can eliminate this approximation by applying the recently derived implicit isometricity of a VAE.

6 CONCLUSION

In this paper, we propose the VAE-SLMC, which makes efficient parallel proposals between modes independent of any previous state, by applying the theoretically derived implicit isometricity of a VAE. In addition, we propose adaptive annealing and parallel exchanging methods that

make the VAE-SLMC applicable to situations where obtaining unbiased training data is difficult. The experimental results show that the proposed method is applicable to various problems having complex multimodal distributions.

We believe that the proposed framework broadens the applications of the SLMC methods in various fields because of its powerful proposals and VAE's versatility. Our method can adopt any kinds of neural networks for the VAE's encoder and decoder, which means that we can benefit from the recent great progress of the deep learning techniques including transfer learning and fine-tuning from a variety of pre-trained models to further improve the performance of the VAE-SLMC.

References

- Albergo, M. S., Kanwar, G., and Shanahan, P. E. (2019). Flow-based generative models for markov chain monte carlo in lattice field theory. *Physical Review D*, 100(3):034515.
- Baumgärtner, A., Burkitt, A., Ceperley, D., De Raedt, H., Ferrenberg, A., Heermann, D., Herrmann, H., Landau, D., Levesque, D., von der Linden, W., et al. (2012). *The Monte Carlo method in condensed matter physics*, volume 71. Springer Science & Business Media.
- Binder, K., Heermann, D., Roelofs, L., Mallinckrodt, A. J., and McKay, S. (1993). Monte carlo simulation in statistical physics. *Computers in Physics*, 7(2):156–157.
- Bobtsov, A. A. and Pyrkun, A. A. (2012). Cancellation of unknown multiharmonic disturbance for nonlinear plant with input delay. *International Journal of Adaptive Control and Signal Processing*, 26(4):302–315.
- Bodson, M. and Douglas, S. C. (1997). Adaptive algorithms for the rejection of sinusoidal disturbances with unknown frequency. *Automatica*, 33(12):2213–2221.
- Duane, S., Kennedy, A. D., Pendleton, B. J., and Roweth, D. (1987). Hybrid monte carlo. *Physics letters B*, 195(2):216–222.
- Foreman-Mackey, D., Hogg, D. W., Lang, D., and Goodman, J. (2013). emcee: the mcmc hammer. *Publications of the Astronomical Society of the Pacific*, 125(925):306.
- Gelman, A., Carlin, J. B., Stern, H. S., and Rubin, D. B. (1995). *Bayesian data analysis*. Chapman and Hall/CRC.
- Han, Q. and Hong, J.-X. (2006). *Isometric embedding of Riemannian manifolds in Euclidean spaces*, volume 13. American Mathematical Soc.
- Hastings, W. K. (1970). Monte carlo sampling methods using markov chains and their applications.
- Higgins, I., Matthey, L., Pal, A., Burgess, C., Glorot, X., Botvinick, M., Mohamed, S., and Lerchner, A. (2016). beta-vae: Learning basic visual concepts with a constrained variational framework.
- Himmelblau, D. M. et al. (2018). *Applied nonlinear programming*. McGraw-Hill.
- Huang, L. and Wang, L. (2017). Accelerated monte carlo simulations with restricted boltzmann machines. *Physical Review B*, 95(3):035105.
- Hukushima, K. and Nemoto, K. (1996). Exchange monte carlo method and application to spin glass simulations. *Journal of the Physical Society of Japan*, 65(6):1604–1608.
- Ihler, A. T., Fisher III, J. W., Moses, R. L., and Willsky, A. S. (2004). Nonparametric belief propagation for self-calibration in sensor networks. In *Proceedings of the 3rd international symposium on information processing in sensor networks*, pages 225–233.
- Inoue, M., Hukushima, K., and Okada, M. (2005). A pca approach to sourlas code analysis. *Progress of Theoretical Physics Supplement*, 157:246–249.
- Inoue, M., Hukushima, K., and Okada, M. (2006). Analysis method combining monte carlo simulation and principal component analysis—application to sourlas code—. *Journal of the Physical Society of Japan*, 75(8):084003.
- Kingma, D. P. and Welling, M. (2013). Auto-encoding variational bayes. *arXiv preprint arXiv:1312.6114*.
- Kirkpatrick, S., Gelatt Jr, C. D., and Vecchi, M. P. (1983). Optimization by simulated annealing. *science*, 220(4598):671–680.
- Kiwata, H. (2019). Deriving the order parameters of a spin-glass model using principal component analysis. *Physical Review E*, 99(6):063304.
- Levy, D., Hoffman, M. D., and Sohl-Dickstein, J. (2017). Generalizing hamiltonian monte carlo with neural networks. *arXiv preprint arXiv:1711.09268*.
- Liu, J., Qi, Y., Meng, Z. Y., and Fu, L. (2017). Self-learning monte carlo method. *Physical Review B*, 95(4):041101.
- Luengo, D., Martino, L., Bugallo, M., Elvira, V., and Särkkä, S. (2020). A survey of monte carlo methods for parameter estimation. *EURASIP Journal on Advances in Signal Processing*, 2020(1):1–62.
- Manly, B. F. (2018). *Randomization, Bootstrap and Monte Carlo Methods in Biology: Texts in Statistical Science*. chapman and hall/CRC.
- Martin, A. D., Quinn, K. M., and Park, J. H. (2011). Mcmc-pack: Markov chain monte carlo in r.
- Monroe, J. I. and Shen, V. K. (2022). Learning efficient, collective monte carlo moves with variational autoencoders. *Journal of Chemical Theory and Computation*.
- Nagata, K. and Watanabe, S. (2008). Asymptotic behavior of exchange ratio in exchange monte carlo method. *Neural Networks*, 21(7):980–988.

- Nakagawa, A., Kato, K., and Suzuki, T. (2021). Quantitative understanding of vae as a non-linearly scaled isometric embedding. In *International Conference on Machine Learning*, pages 7916–7926. PMLR.
- Neal, R. M. et al. (2011). Mcmc using hamiltonian dynamics. *Handbook of markov chain monte carlo*, 2(11):2.
- Rastrigin, L. A. (1974). Systems of extremal control. *Nauka*.
- Rolinek, M., Zietlow, D., and Martius, G. (2019). Variational autoencoders pursue pca directions (by accident). In *Proceedings of the IEEE/CVF Conference on Computer Vision and Pattern Recognition*, pages 12406–12415.
- Roussel, C., Cocco, S., and Monasson, R. (2021). Barriers and dynamical paths in alternating gibbs sampling of restricted boltzmann machines. *Physical Review E*, 104(3):034109.
- Shen, H., Liu, J., and Fu, L. (2018). Self-learning monte carlo with deep neural networks. *Physical Review B*, 97(20):205140.
- Shlens, J. (2014). A tutorial on principal component analysis. *arXiv preprint arXiv:1404.1100*.
- Silagadze, Z. (2007). Finding two-dimensional peaks. *physics of Particles and Nuclei Letters*, 4(1):73–80.
- So, H.-C., Chan, K. W., Chan, Y. T., and Ho, K. (2005). Linear prediction approach for efficient frequency estimation of multiple real sinusoids: algorithms and analyses. *IEEE Transactions on Signal Processing*, 53(7):2290–2305.
- Sohl-Dickstein, J., Mudigonda, M., and DeWeese, M. (2014). Hamiltonian monte carlo without detailed balance. In *International Conference on Machine Learning*, pages 719–726. PMLR.
- Stoica, P. (1993). List of references on spectral line analysis. *Signal Processing*, 31(3):329–340.
- Swendsen, R. H. and Wang, J.-S. (1986). Replica monte carlo simulation of spin-glasses. *Physical review letters*, 57(21):2607.
- Tanaka, A. and Tomiya, A. (2017). Towards reduction of autocorrelation in hmc by machine learning. *arXiv preprint arXiv:1712.03893*.
- Wang, L. (2016). Discovering phase transitions with unsupervised learning. *Physical Review B*, 94(19):195105.
- Woodard, D., Schmidler, S., and Huber, M. (2009). Sufficient conditions for torpid mixing of parallel and simulated tempering. *Electronic Journal of Probability*, 14:780–804.
- Xu, X. Y., Qi, Y., Liu, J., Fu, L., and Meng, Z. Y. (2017). Self-learning quantum monte carlo method in interacting fermion systems. *Physical Review B*, 96(4):041119.

Toward Unlimited Self-Learning Monte Carlo with Annealing Process Using VAE’s Implicit Isometricity: Supplementary Materials

A OVERVIEW

This supplementary material provides extended explanations, implementation details, and additional results for the paper “Toward Unlimited Self-Learning Monte Carlo with Annealing Process Using VAE’s Implicit Isometricity.”

B EXTENDED EXPLANATIONS OF VAE’S IMPLICIT ISOMETRICITY

In this section, we show how to check the consistency of the VAE’s implicit isometricity shown in the paper and how to efficiently analyze the properties of probability distributions from the obtained samples using the implicit isometricity.

B.1 Checking Isometricity of the VAE

This section explains the implicit isometric property of a VAE and shows how to check whether a VAE acquires the isometricity.

First, Rolinek et al. (2019) both theoretically and experimentally show that an arbitrary pair of column vectors in the Jacobian matrix $\partial x / \partial \mu_{m,\phi}(x)$ are orthogonal. Nakagawa et al. (2021) further show that VAEs have an implicit isometric property,

$$\frac{2\sigma_{m,\phi}^2(x)}{\beta_{\text{VAE}}} \left(\frac{\partial x}{\partial \mu_{m,\phi}(x)} \right)^\top G_x \left(\frac{\partial x}{\partial \mu_{n,\phi}(x)} \right) = \delta_{mn}, \quad \forall m, n \in \{1, \dots, M\}, \quad (9)$$

where G_x and δ_{mn} denote a metric tensor derived from $p_\theta(x|z)$ and the Kronecker delta, respectively. In the case $p_\theta(x|z) = \mathcal{N}(x; \hat{x}, 2I_D)$, where \hat{x} denotes a decoded value of z , the reconstruction loss in the VAE objective becomes the sum of squared errors (SSE) and the metric tensor G_x becomes an identity matrix I_M . In this case, $|\det(\partial \mu_\phi(x) / \partial x)| \propto \prod \sigma_{m,\phi}(x)$ holds from Eq. (9). Thus Eq. (4) in the main text holds by using $p_\theta(x) = |\det(\partial \mu_\phi(x) / \partial x)| p(\mu_\phi(x))$.

Then we explain the evaluation method of whether VAE captures the isometricity. In the following discussion, we assume that the SSE metric is used as a reconstruction loss of the VAE objective. From Eq. (9) and $G_x = I_M$, a property

$$\sqrt{\frac{2\sigma_{m,\phi}^2(x)}{\beta_{\text{VAE}}}} \left\| \frac{\partial x}{\partial \mu_{m,\phi}(x)} \right\|_2 = 1 \quad (10)$$

holds in each latent dimension m if th VAE satisfies Eq. (9).

Eq. (10) can be numerically estimated as

$$\sqrt{\frac{2\sigma_{m,\phi}^2(x)}{\beta_{\text{VAE}}}} \left\| \frac{\partial x}{\partial \mu_{m,\phi}(x)} \right\|_2 \simeq \sqrt{\frac{2\sigma_{m,\phi}^2(x)}{\beta_{\text{VAE}}} \frac{\|\text{Dec}_\theta(\mu_\phi(x)) - \text{Dec}_\theta(\mu_\phi(x) + \Delta e_{(m)})\|_2}{\Delta}}, \quad (11)$$

where $\text{Dec}_\theta : \mathbb{R}^M \rightarrow \mathbb{R}^D$ is a trained VAE decoder, Δ is an infinitesimal constant for numerical differentiation, and $e_{(m)}$ is a one-hot vector $(0, \dots, 1, \dots, 0)$, in which only the m -th dimensional component is 1 and the others are 0. We define the isometric factor for each latent dimension as

$$\text{Iso}_m = \mathbb{E}_{p_{\mathcal{D}}} \left[\sqrt{\frac{2\sigma_{m,\phi}^2(x)}{\beta_{\text{VAE}}} \frac{\|\text{Dec}_\theta(\mu_\phi(x)) - \text{Dec}_\theta(\mu_\phi(x) + \Delta e_{(m)})\|_2}{\Delta}} \right], \quad (12)$$

where $\mathbb{E}_{p_{\mathcal{D}}}$ denote the average value over the generated 100,000 samples from p_θ . If the isometric factor is close to 1, the probability $p_\theta(x)$ can be correctly estimated by using Eq. (4) in the main document. Note that the orthogonality holds as shown in Nakagawa et al. (2021); Rolinek et al. (2019).

Table 2: Evaluation of the isometric factors Iso_m in the trained VAE models

Latent dim. m	GMM-2	GMM-3	GMM-4	GMM-5	ICG	BABABA	SCG	RW
1	0.974	0.978	0.996	0.987	1.009	1.009	1.000	0.999
2	0.986	0.987	0.990	0.990	1.013	0.993	1.003	1.000
3	0.990	0.987	0.990	0.992	1.013			
4	0.987	0.991	0.999	0.994	1.012			
5	0.993	0.993	0.992	0.996	1.000			
6	0.992	0.993	1.000	0.992	1.019			
7	0.992	0.995	0.996	0.991	1.014			
8	1.001	0.992	1.000	0.990	1.013			
9	0.999	1.004	1.001	0.995	1.004			
10	1.002	1.004	0.993	0.997	1.025			

Table 2 shows the isometric factor Iso_m of each dimension m of the VAE latent variable in a descending order of the importance calculated by Eq. (13). Δ in Eq. (12) is set to 0.001. GMM-[2, 3, 4, 5] show Gaussian Mixtures ($D = 10, M = 10$) with [2, 3, 4, 5] clusters used in Sec. 4.1 in the main text. ICG is Ill-Conditional Gaussian ($D = 100, M = 100$) explained in Section D.2. For ICG, top 10-dimensional values from 100 dimensions are listed in the table. BANANA ($D = 2, M = 2$), SCG ($D = 2, M = 2$), and RW ($D = 2, M = 2$) denote banana-shaped density, strongly correlated Gaussian, and rough well distributions, respectively, as explained in Sec. D.2. See Sec. E for details of the experiment conditions. As shown in this table, the isometric factors for each dimension in our experiments are very close to 1.0, showing the proposal probability can be correctly estimated from Eq. (4) in the main document.

B.2 Understanding the Structure of Probability Distributions

By using the properties of VAE, the structure of probability distributions can be analyzed at low cost. In Bayesian statistics and other probabilistic inference, principal component analysis (PCA) (Shlens, 2014) of the samples generated by a sampling method such as MCMC methods is sometimes performed to understand the structure of probability distribution (Inoue et al., 2005, 2006; Wang, 2016; Kiwata, 2019). However, the computational cost for calculating eigenvalues in PCA is $\mathcal{O}(\min(D^3, P^3))$, where D is the data dimension and P is the number of samples generated by an MCMC method. However, by using the VAE obtained by VAE-SLMC, a low-dimensional compression similar to PCA is possible just by encoding and decoding the samples with a cost of $\mathcal{O}(\Lambda D)$, where Λ is a computational cost of a VAE’s encoder. The importance of each latent dimension $m = 1, \dots, M$ in the latent space can be evaluated (Nakagawa et al., 2021) as

$$\kappa_m = \frac{\beta}{2} \mathbb{E}_{p_\theta} [1/\sigma_{m,\phi}^2(x)]. \tag{13}$$

We substitute \mathbb{E}_{p_θ} for the empirical mean of P samples and encoded variance $\sigma_\phi(x) = (\sigma_{m,\phi})_{m=1}^M$ can be obtained by passing P samples through encoder-decoder.

C ALGORITHM DETAILS

In this section, we describe the implementation details of the proposed VAE-SLMC with adaptive annealing and parallel annealing methods.

C.1 Summary of the Proposed VAE-SLMC Methods

Here, we summarize the variation of the proposed VAE-ALMC methods. Table 3 lists all the combinations of the proposed method with the adaptive annealing technique (in Sec. 3.3 and Algorithms 3 and 4) and the parallel annealing exchange technique (in Sec. 3.4 and Algorithms 5 and 6). The abbreviations of the algorithms (CA-VAE-SLMC, AA-VAE-SLMC, CA-VAE-ESLMC, and AA-VAE-ESLMC) used in the experiments are also described. “CA-” means constant annealing, which is a method without adaptive annealing.

Table 3: Experimental Conditions, Abbreviations, and Algorithms used in each Conditions

Method	VAE-SLMC (Sec. 3.1) (Alg. 1)	Annealing (Sec. 3.2) (Alg. 2)	Adaptive annealing (Sec. 3.3) (Alg. 3 and 4)	Parallel annealing exchange (Sec. 3.4) (Alg. 5 and 6)
Naïve VAE-SLMC	✓			
CA-VAE-SLMC	✓	✓		
AA-VAE-SLMC	✓	✓	✓	
CA-VAE-ESLMC	✓	✓		✓
AA-VAE-ESLMC	✓	✓	✓	✓

Algorithm 3 Adaptive Annealing VAE-SLMC

Input a target distribution $\tilde{p}(x; \beta)$, an initial β_0 , training data \mathcal{D}_0 , an initial model $p_{\theta_0}(x; \beta_0)$, an initial distribution π_0 .

- 1: Initialize $x^{(0)} \sim \pi_0$
- 2: **for** $k = 1$ to K **do**
- 3: $\beta_k = \text{BETA-SEARCH}(\beta_{k-1}; \text{AR}_{\min}, \text{AR}_{\max}, \varepsilon, \{\beta'_{(s)}\}_{s=0}^S, T_{\max}, \mathcal{D}_{k-1})$ ▷ See Algorithm 4
- 4: Set $(x_k^{(t)})_{t=0}^T = \text{VAE-SLMC}(\tilde{p}(x; \beta_k), p_{\theta_{k-1}}(x; \beta_{k-1}), \Gamma_{\theta_{k-1}}(x; \beta_{k-1}); T, T_{\text{train}}, \pi_0, \mathcal{D}_{k-1})$ from Algorithm 1.
- 5: Make the training data \mathcal{D}_k from $(x_k^{(t)})_{t=0}^T$
- 6: Train p_{θ_k} with \mathcal{D}_k
- 7: **end for**
- 8: Set $(x_K^{(t)})_{t=0}^T = \text{VAE-SLMC}(\tilde{p}(x; \beta_K), p_{\theta_K}(x; \beta_K), \Gamma_{\theta_K}(x; \beta_K); T, T_{\text{train}}, \pi_0, \mathcal{D}_K)$

Output samples $(x_K^{(t)})_{t=0}^T$

C.2 Adaptive Annealing VAE-SLMC

Algorithm 3 illustrates the steps of adaptive annealing VAE-SLMC (AA-VAE-SLMC) explained in Sec. 3.3 of the main text. The details the input of Alogorithm 3 are as follows:

- A target distribution $p(x; \beta) \propto \tilde{p}(x; \beta)$: This denotes a probability distribution from which a user wishes to sample. The normalizing factor is not necessary to compute acceptance probability.
- An initial β_0 : The inverse temperature where the annealing process starts. β_0 should be set so that the probability distribution is easily explorable even with a local update MCMC method.
- Training data \mathcal{D}_0 : Training data used to train the initial model $p_{\theta_0}(x; \beta_0)$.
- An initial model $p_{\theta_0}(x; \beta_0)$: A model trained with the training data \mathcal{D}_0 .
- An initial distribution π_0 : An initial distribution of VAE-SLMC during annealing. In simulated annealing, it is necessary to simulate the β_k probability distribution with the final state of the simulation of the β_{k-1} probability distribution as the initial value $x_k^{(0)}$ because the transition between modes becomes more difficult as the inverse temperature is large. However, VAE-SLMC works for arbitrary initial distributions because the proposal is independent of previous states, and transitions between modes are easy. Therefore, the algorithm uses the same initial distribution for all k without loss of generality.

In all the numerical experiments, we set $T_{\text{train}} = \infty, \forall k \in \{1, \dots, K\}$ in order not to perform the retraining steps in the VAE-SLMC process in from Algorithm 1.

In Line 3 of Algorithm 3, β is adaptively determined by Algorithm 4, whose inputs are detailed as follows:

- β : A current value of β .
- $\text{AR}_{\min}, \text{AR}_{\max}$: Upper and lower bounds for the acceptance rate of the VAE-SLMC at each annealing step. The upper and lower bounds are the values determined by a user according to the acceptance rate sought at the end of the annealing process $\beta_K = 1$. For a typical behavior of the lower and upper bounds of the adaptive annealing VAE-SLMC, please refer to Sec. D.3.

Algorithm 4 Adaptive β determination

```

1: function BETA-SEARCH( $\beta$  ;  $AR_{\min}$ ,  $AR_{\max}$ ,  $\varepsilon$ ,  $\{\beta'_{(s)}\}_{s=0}^S$ ,  $T_{\max}$ ,  $T_{\text{check}}$ ,  $\mathcal{D}$ )
2:   for  $t = 1$  to  $T_{\max}$  do
3:     Calculate  $\{AR(\beta'_{(s)})\}_{s=0}^S$  by VAE-SLMC( $\tilde{p}(x; \beta'_{(s)})$ ,  $p_{\theta_\beta}(x; \beta)$ ,  $\Gamma_{\theta_\beta}(x; \beta)$ ;  $T_{\text{check}}$ ,  $T_{\text{train}}$ ,  $\pi_0$ ,  $\mathcal{D}$ )   ▷ Parallel
       search
4:     if  $\exists AR_{\min} \leq AR(\beta'_{(s)}) \leq AR_{\max}$ ,  $\forall s \in \{0, \dots, S\}$  then
5:       Select  $\beta'_{(s)}$  from  $\{\beta'_{(s)} \mid AR_{\min} \leq AR(\beta'_{(s)}) \leq AR_{\max}, \forall s \in \{0, \dots, S\}\}$ .
6:       break
7:       return  $\beta'_{(s)}$ 
8:     else                                                                                               ▷ Sequential search
9:       if  $AR(\beta_s) \leq AR_{\min}$ ,  $\forall s \in \{0, \dots, S\}$  then
10:         $\beta'_{(s)} \leftarrow \beta'_{(s)} - \varepsilon$ ,  $\forall s \in \{0, \dots, S\}$ 
11:       else
12:         $\beta'_{(s)} \leftarrow \beta'_{(s)} + \varepsilon$ ,  $\forall s \in \{0, \dots, S\}$ 
13:
14:       end if
15:     end if
16:   end for
17:   return  $\beta'_{(s)}$ 
18: end function

```

- ε : A parameter used to update the candidates $\{\beta'_{(s)}\}_{s=0}^S$ in a sequential search step.
- $\{\beta'_{(s)}\}_{s=0}^S$: An initial sequence of β candidates $\{\beta'_{(s)}\}_{s=0}^S$. They consist of the input β and smaller and larger values around β with a user-defined granularity, e.g., an equal interval or a logarithmically equal interval.
- T_{\max} : The maximum number of iterations for sequential β search.
- T_{check} : The number of the Monte Carlo steps in VAE-SLMC used to estimate acceptance rates of the β candidates $\{\beta'_{(s)}\}_{s=0}^S$.

The followings are additional notes with respect to Algorithm 4:

Parallel calculation of acceptance rates. In order to calculate the acceptance rates of candidates $\{\beta'_{(s)}\}_{s=0}^S$ in Line 3 by a local update MCMC method, it is necessary to calculate the acceptance rate by S times local update MCMC simulations. Computation of the acceptance rates in Line 3 can be executed in parallel since SLMC proposes candidates independent of the previous state. In other words, the overhead of calculating the acceptance rates for S candidates by using SLMC only changes the number of calculating acceptance rates from 1 to S for each step of VAE-SLMC.

Selection from β candidates. In Line 5, if there are multiple β_s that satisfy the conditions, you can select $\beta'_{(s)}$ according to arbitrary rules. For example, if you select the largest β among all the β_s satisfying the condition, the number of annealing steps will be small, but the acceptance rate will be about the lower bound. On the other hand, if you select the smallest β among all the β_s satisfying the conditions, the number of annealing steps will be larger, but the acceptance rate will be about the upper bound.

C.3 Parallel Annealing Exchange VAE-SLMC

Algorithm 5 illustrates the steps of parallel annealing exchange VAE-SLMC (CA-VAE-ESLMC) explained in Sec. 3.4 of the main text. The details the input of Algorithm 5 are as follows:

- A target distribution $p(x; \beta) \propto \tilde{p}(x; \beta)$: This denotes a probability distribution from which a user wishes to sample. The normalizing factor is not necessary to compute acceptance probability.
- A β -sequence $\{\beta_k^j\}_{k=0, \dots, K}^{j=0, \dots, J}$: A set of β s to determine the annealing schedules for all the parallel chains. j and k indices represent the parallel chains and the annealing steps, independently. We set up the sequence of inverse

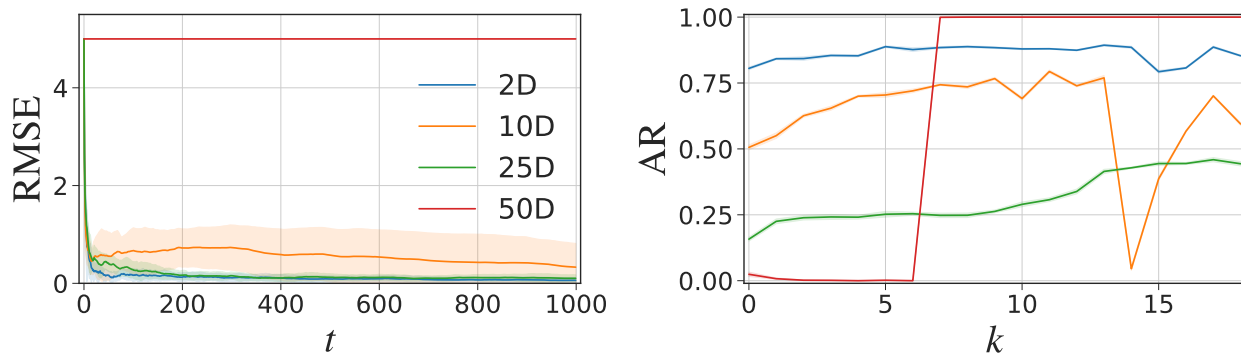


Figure 9: The result of CA-VAE-SLMC simulation with $\{\beta_k = \beta_0 + k\Delta\beta \mid \beta_{20} = 1.0\}_{k=0}^{20}$ on three-cluster Gaussian mixture with dimensions $D = [2, 10, 25, 50]$. (Left) RMSE after t -th Monte Carlo step and (Right) the acceptance rate (AR) estimated by 50,000 Monte Carlo steps as a function of the annealing steps k .

temperatures $\{\beta_0^j\}_{j=0}^J$, $\beta_0^0 \geq \dots \geq \beta_0^J$ so that the inverse temperatures are well exchanged between the chains and β_0 in such a way that a local update EMC method can easily explore.

- An initial model $\{p_{\theta_0^j}(x; \beta_0^j)\}_{j=0}^J$: A model trained with the training data $\{\mathcal{D}_0^j\}_{j=0}^J$ from $\{p(x; \beta_0^j)\}_{j=0}^J$ by a local update EMC method.
- Training data $\{\mathcal{D}_0^j\}_{j=0}^J$: Training data used to train the initial model $\{p_{\theta_0^j}(x; \beta_0^j)\}_{j=0}^J$.
- An initial distribution π_0 : An initial distribution of VAE-ESLMC during annealing. We use the same initial distribution in the annealing process for the same reasons as described in Sec. C.2.

In Line 3 of Algorithm 5, samples are generated by VAE-ESLMC described in Algorithm 6), which uses the same exchange process as the replica exchange Monte Carlo method (Hukushima and Nemoto, 1996). For all parallel chains, the exchange probability is defined as Eq. (7). The same “retrain” step as in VAE-SLMC can also be incorporated into the VAE-ESLMC. However, retraining is not performed in all numerical experiment (i.e., $T_{\text{train}} = \infty$).

D ADDITIONAL RESULTS

In this section, we report additional results omitted from the main text because of limited space.

D.1 Failure Behavior of CA-VAE-SLMC

The results of annealing VAE-SLMC are sensitive to how the β sequence is determined. Simply setting a constant-interval β sequence $\{\beta_0 + k\Delta\beta\}_{k=0}^{K-1}$ often results in inaccurate samples because of a lack of model learning. Figure 9 shows a failure behavior of CA-VAE-SLMC using Algorithm 2 with a β sequence $\{\beta_k = 0.1 + k\Delta\beta \mid \beta_{20} = 1.0\}_{k=0}^{20}$, $T_{\text{train}} = \infty$ (i.e., no retrain steps, $\mathcal{D} = \emptyset$) and $\pi_0 = \delta(x - (5, \dots, 5))$ without loss of generality. For the initial training of the VAE, we use 40,000 training data at $\beta_0 = 0.1$ by a local update MCMC method. The RMSE should decrease for Monte Carlo steps t , and the AR should be higher if possible. First, the 2D and 25D results show that the acceptance rate increases as annealing proceeds. This suggests a pre-training effect as described in the main text Sec. 3.2. On the other hand, in 10D, we can see that the acceptance rate decreases sharply in the middle of annealing. This may be due to over- or under-learning the model in the middle of annealing or inappropriate beta intervals. Furthermore, in 50D, the acceptance rate becomes almost zero at the beginning, and the VAE in the middle of annealing learns only a part of the distribution. As a result, only a part of the support of the distribution is learned well, and the acceptance rate approaches 1, but biased samples are generated, and the RMSE does not decrease. These result are typical phenomenon observed not only in the specific case but also throughout the present numerical experiments, suggesting that the CA-VAE-SLMC is unstable and that adaptively determining the β is important.

Algorithm 5 Parallel Annealing VAE-ESLMC

Input a target distribution $\tilde{p}(x)$, a β -sequence $\{\beta_k^j\}_{k=0,\dots,K}^{j=0,\dots,J}$, an initial models $\{p_{\theta_0^j}(x; \beta_0^j)\}_{j=1}^J$, an initial distribution π_0 , training data $\{\mathcal{D}_0^j\}_{j=0}^J$

- 1: Initialize $\{x^{j,(0)}\}_{j=0}^J \sim \pi_0$
- 2: **for** $k = 1$ to K **do**
- 3: Set $\{(x_k^{j,(t)})\}_{j=1}^J = \text{VAE-ESLMC}(\{\tilde{p}(x; \beta_k^j)\}_{j=1}^J, \{p_{\theta^j}(x; \beta_{k-1}^j)\}_{j=0}^J, \{\Gamma_{\theta_{k-1}^j}(x; \beta_{k-1}^j)\}_{j=0}^J, \{\beta_k^j\}_{j=0}^J;$
 $T, T_{\text{train}}, \{\mathcal{D}_{k-1}^j\}_{j=0}^J, \pi_0)$ ▷ See Algorithm. 6
- 4: Make the training data $\{\mathcal{D}_k^j\}_{j=0}^J$ from $\{(x_k^{j,(t)})\}_{j=1}^J$.
- 5: Train $\{p_{\theta_k^j}(x; \beta_k^j)\}_{j=0}^J$ with $\{\mathcal{D}_k^j\}_{j=0}^J$
- 6: **end for**
- 7: Set $\{(x_K^{j,(t)})\}_{j=1}^J = \text{VAE-ESLMC}(\{\tilde{p}(x; \beta_K^j)\}_{j=1}^J, \{p_{\theta_K^j}(x; \beta_K^j)\}_{j=0}^J, \{\Gamma_{\theta_K^j}(x; \beta_K^j)\}_{j=0}^J, \{\beta_K^j\}_{j=0}^J;$
 $T, T_{\text{train}}, \{\mathcal{D}_K^j\}_{j=0}^J, \pi_0)$

Output samples $(x_K^{(t),j})_{t=0}^T$

Algorithm 6 VAE-ESLMC

- 1: **function** VAE-ESLMC($\{\tilde{p}(x; \beta^j)\}_{j=0}^J, \{p_{\theta^j}(x; \beta^j)\}_{j=0}^J, \{\Gamma_{\theta^j}(x; \beta^j)\}_{j=0}^J, \{\beta^j\}_{j=0}^J; T, T_{\text{train}}, \{\mathcal{D}^j\}_{j=0}^J, \pi_0)$
- 2: Initialize $x^{(0)} \sim \pi_0$
- 3: **while** $t \leq T$ **do**
- 4: **for** $j = 0$ to J **do**
- 5: Generate $x'^{j} \sim p_{\theta^j}(x; \beta^j)$
- 6: Calculate $A(x'^{j} | x^{(t),j})$ by Eq. (5) in main text
- 7: **if** $(A(x' | x^{(t)}) > U[0, 1])$ **then**
- 8: $x^{(t+1),j} \leftarrow x'^{j}$
- 9: **else**
- 10: $x^{(t+1),j} \leftarrow x^{(t),j}$
- 11: **end if**
- 12: **if** $t \equiv 0 \pmod{T_{\text{train}}}$ **then** ▷ Retrain Step
- 13: Make training data $\mathcal{D}^{(t)}$ from $(x^{(t)})_{t=0}^t$
- 14: Set $\mathcal{D}^j \leftarrow \mathcal{D}^j \cup \mathcal{D}^{(t),j}$
- 15: Train $p_{\theta^j}(x^j; \beta^j)$ with \mathcal{D}^j and update $\Gamma_{\theta^j}(x^j; \beta^j)$ ▷ Use the last parameters as initial parameters for training
- 16: **end if**
- 17: **end for**
- 18: Select $x^{(t),j} \in \{x^{(t),j}\}_{j=0}^J$
- 19: Calculate $A_{\text{ex}}(x^{(t),j+1}, x^{(t),j})$ by Eq. (7)
- 20: **if** $A_{\text{ex}}(x^{(t),j+1} | x^{(t),j}) > U[0, 1]$ **then**
- 21: $x^{(t),j} \leftarrow x^{(t),j+1}$
- 22: $x^{(t),j+1} \leftarrow x^{(t),j}$
- 23: **end if**
- 24: $t \leftarrow t + 1$
- 25: **end while**
- 26: **return** samples $(x^{(t),j})_{t=0,\dots,T}^{j=0,\dots,J}$
- 27: **end function**

Table 4: Effective sample size (ESS) for the naïve VAE-SLMC and HMC. ESS depends on the statistic being estimated; we compute it for the 1st moment and 2nd moment of each dimension and report the minimum across statistics and dimensions of the mean ESS across 10 runs for the naïve VAE-SLMC and HMC, report \pm standard errors; see the supplementary material for the behaviors of the autocorrelation function.

Target	HMC	Naïve VAE-SLMC
Ill-conditioned Gaussian (100D)	$2.58 \times 10^{-2} \pm 8.02 \times 10^{-4}$	$5.20 \times 10^{-1} \pm 9.46 \times 10^{-3}$
Strongly correlated Gaussian (2D)	$1.50 \times 10^{-2} \pm 7.11 \times 10^{-4}$	$9.65 \times 10^{-1} \pm 7.62 \times 10^{-3}$
Banana-shaped density (2D)	$9.32 \times 10^{-2} \pm 1.66 \times 10^{-3}$	$2.30 \times 10^{-1} \pm 3.69 \times 10^{-3}$
Rough well density (2D)	$5.22 \times 10^{-4} \pm 1.96 \times 10^{-4}$	$3.89 \times 10^{-3} \pm 9.24 \times 10^{-4}$

D.2 Experiments of Naïve VAE-SLMC

In this section, we show that even the naïve VAE-SLMC can generate samples more efficiently than HMC, the most common method for continuous probability distributions when good training data can be obtained. We evaluate the performance of the naïve VAE-SLMC which uses only Algorithm 1, i.e., without annealing, on the following toy test distributions:

- Ill-conditioned Gaussian (ICG): A 100-dimensional multivariate normal distribution with mean 0 and variance Σ . Eigenvalues of Σ range from 10^{-2} to 10^2 and eigenvectors are chosen in a random orthonormal basis.
- Strongly correlated Gaussian (SCG): A diagonal 2-dimensional normal distribution with variance $[10^2, 10^{-2}]$ rotated by $\pi/4$. This is an extreme version of the example by Neal et al. (2011).
- Banana-shaped density (BANANA): A 2-dimensional probability distribution as

$$x_1 \sim \mathcal{N}(0, 10); \quad x_2 \sim \mathcal{N}(0.03(x_1^2 - 100), 1).$$

This distribution has a strong ridge-like geometrical structure that is difficult for HMC (Duane et al., 1987) to understand its structure.

- Rough well density (RW): A distribution similar to the example by Sohl-Dickstein et al. (2014), for a given $\eta > 0$,

$$p(x) \propto \exp\left(-\frac{1}{2}x^\top x + \eta \sum_{i=1}^n \cos\left(\frac{x_i}{\eta}\right)\right).$$

For a small η , the distribution itself does not change much, but the surface is perturbed by high-frequency tines oscillating between -1 and 1 . In our numerical experiments, we set $\eta = 10^{-2}$.

For each of them, we compare the naïve VAE-SLMC with Hamilton Monte Carlo (HMC) (Duane et al., 1987) which fix 10 leapfrog steps and use well-tuned step size. We also set $n(\mathcal{D}) = 20,000$ to train a VAE. The samples used as training data were generated by well-tuned HMC and spaced long enough to be almost independent samples; see Supplementary Materials Sec. E.4 for details of parameters of HMC. In this numerical experiment, the performance of VAE-SLMC is evaluated by ESS, which is commonly used in HMC evaluations (Levy et al., 2017), instead of RMSE. Specifically, we measured performance via the mean across runs of the minimum effective sample size (ESS) across dimensions and the 1st and 2nd order moments, motivated by Levy et al. (2017); see Supplementary Materials Sec. E.5 for details of definition and meaning. Table 4 summarizes the results for the distributions. The naïve VAE-SLMC performs well in the experiments. This result indicates that MCMC can be significantly accelerated if a good sequence of samples is obtained by some method.

D.3 Dependency of AR_{\min} in Algorithm 3

Figure 10 shows the dependency of the lower bound AR_{\min} in AA-VAE-SLMC on the annealing β and the acceptance rate denoted on the colorbar after k -th annealing step, and the RMSEs after t -th Monte Carlo step in three-cluster 10D Gaussian, which are the same settings used in the main text Sec. 4.1 except for lower bound AR_{\min} . This result confirms that the acceptance rate AR falls appropriately between the upper bound $AR_{\max} = 1.0$ and lower bounds.

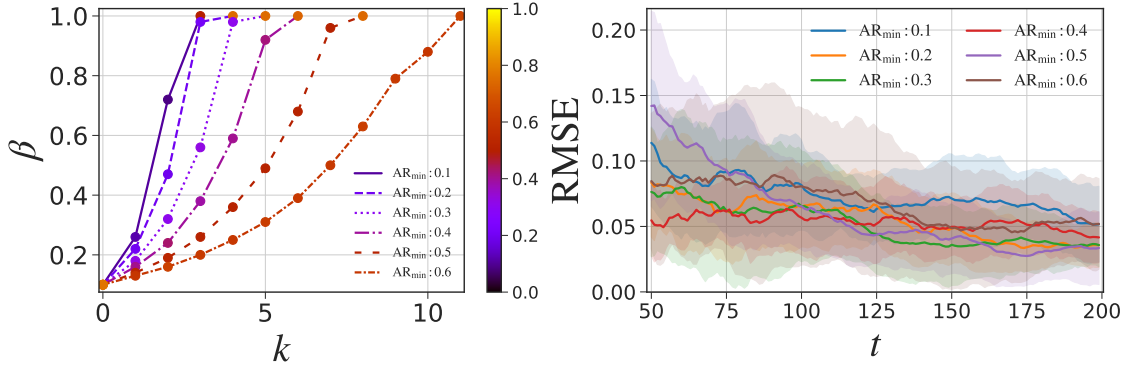


Figure 10: Dependence of the lower bound AR_{\min} on the β transition, the acceptance rate, and RMSE in a three-cluster 10D Gaussian. (Left) The β transition after k -th annealing, and acceptance rates for all AR_{\min} . The colorbar denotes the acceptance rate. (Right) RMSE after t -th Monte Carlo step.

From these results, a large value of AR_{\min} requires a long number of annealing processes to reach $\beta_K = 1$, while a small value of AR_{\min} results in a small number of annealing processes to reach $\beta_K = 1$. Specifically, when $AR_{\min} = 0.6$, 11 times of annealing processes ($K = 11$) are required to reach $\beta_K = 1$, but when $AR_{\min} = 0.1$, only 3 times of annealing process ($K = 3$) are required. We also find that for any given AR_{\min} , the RMSE decreases as same, indicating that the algorithm works for any given AR_{\min} . Furthermore, when AR_{\min} is between 0.1 and 0.5, the last beta intervals become smaller because $\beta_K = 1.0$, and the acceptance rates increase rapidly. This result suggests that it is effective to set AR_{\min} to a low value, reduce the number of the annealing process, and retrain at the end.

D.4 Sensor Network Localization

In this section, we examine the results of AA-VAE-SLMC applied to the problem to estimate the location of a sensor network by Bayesian estimation. This problem is typically a multimodal posterior distribution with multiple modes; see Supplementary Material Sec. E for details of parameter settings of the AA-VAE-SLMC. Specifically, we follow the experimental setup by Ihler et al. (2004) and assume that N sensors have two-dimensional locations denoted by $\{x^{(s)} \in \mathbb{R}^2\}_{s=1}^N$ and exist in a two-dimensional plane. The distance $(x^{(s)}, x^{(s')})$ between a pair of sensors is observed with probability $p(x^{(s)}, x^{(s')}) = \exp(-0.5\|x^{(s)} - x^{(s')}\|^2/R^2)$, and the distance follows $d_{s,s'} = \|x^{(s)} - x^{(s')}\| + \varepsilon$, $\varepsilon \sim \mathcal{N}(0, \sigma_\varepsilon)$ including Gaussian noise. Given a set of observations $d_{s,s'}$ and a prior (uniform distribution) of $x^{(s)}$, a typical task is to infer all sensor positions from the posterior distribution. We set $N = 8$ ($D = 16$), $R/L = 0.3$, $\sigma_\varepsilon/L = 0.02$, and add three sensors with known positions. The positions of eight sensors form a 16-dimensional multimodal distribution. This distribution is difficult for a local updated MCMC method to visit all the modes, and a large bias is introduced to the obtained samples. Convergence is evaluated using the relative error of the estimated mean (REM) in all dimensions. The REM is a summary of the error in approximating the expected value of a variable across all dimensions, which is computed as

$$REM_t = \frac{\sum_{i=1}^{2N} |\bar{x}_i^{(t)} - x_i^*|}{\sum_{i=1}^{2N} |x_i^*|}, \quad (14)$$

where $\bar{x}_i^{(t)} = \sum_{\tau=1}^t x_i^{(\tau)} / \sum_{\tau=1}^t 1$ and denote the sampling average of the i -th variable at time t . Moreover, x_i^* is the mean of the i -th variable of the target probability distribution. We first train the VAE with 40,000 training data at $\beta_0 = 0.1$, which are generated using a local updated MCMC method with the acceptance rate tuned to almost in a range between 0.2 and 0.3. AA-VAE-SLMC start from $\beta_0 = 0.1$ and, we set $AR_{\min} = 0.15$, $AR_{\max} = 1.0$, $\varepsilon = 0.01$; adaptive β from $\beta' = 1.0$ at each β' proposal step. The left side of Fig. 11 shows the dynamics of the REM and the right side of Fig. 11 shows known and unknown sensor positions and generated samples by AA-VAE-SLMC on two-dimensional planar.

The REM rapidly decreases for samples with a fast transition between multiple modes and small autocorrelation (see Sec. E.5). The figure on the left shows that AA-VAE-SLMC has a much more rapidly decreasing REM than MH-EMC, which suggests that the VAE obtained by annealing is proposing between modes at high speed, producing samples with much smaller autocorrelations. The figure on the right shows that multiple modes of the posterior distribution can be

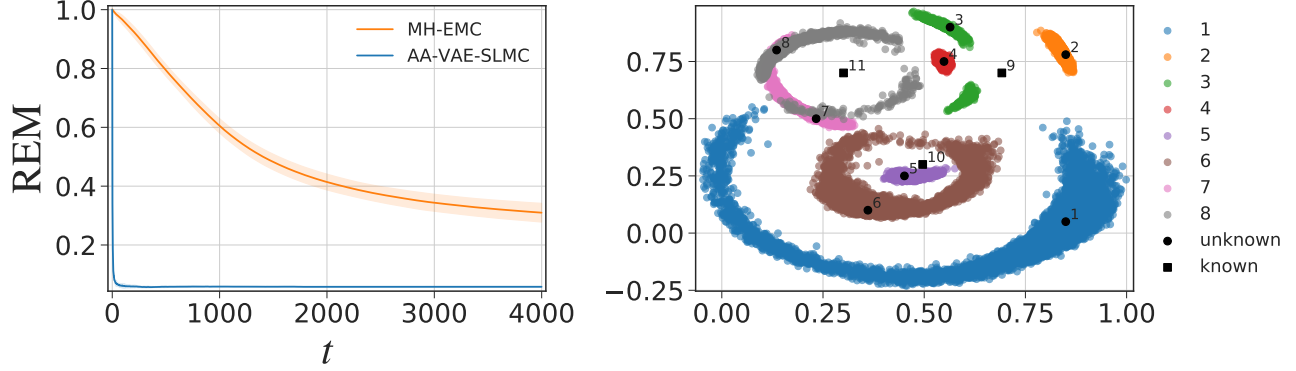


Figure 11: The relative error of the estimated mean (REM). The mean and standard deviation are computed from 10 Markov chain at $\beta_k = 1.0$ with AA-VAE-SLMC. (Left) The horizontal axis indicates Monte Carlo steps. (Right) The square vertices represent the two-dimensional planar positions of known sensors, and the circle vertices represent the two-dimensional planar positions of unknown sensors. The scatter plots represent the sample sequences generated by AA-VAE-SLMC.

sampled precisely centered on the true position of the unknown sensor.

D.5 Additional Optimization Problems

We validate the performance of AA-VAE-SLMC for more optimization problems in addition to that of in Sec. 4.3 in the main text. We use three standard benchmark test functions: Himmelblau function (Himmelblau et al., 2018), Rastrigin function (Rastrigin, 1974), and Styblinski–Tang function (Silagadze, 2007). See Supplementary Material Sec. E for details of the parameter setting for AA-VAE-SLMC.

- Himmelblau function: A multimodal function with four global optimal solutions:

$$f(x) = (x_1^2 + x_2 - 11)^2 + (x_1 + x_2^2 - 7)^2,$$

subject to $x_i \in [-6, 6]$. The global minimum is located at

$$x^* = (3, 2), (-2.8051118, 3.283186), (-3.779310, -3.283186), (3.584458, -1.848126), \quad f(x^*) = 0.$$

- Rastrigin function: A function that has a global optimal solution at the origin, where the function value is zero, defined by

$$f(x) = \sum_{i=1}^D (x_i^2 - 10 \cos(2\pi x_i)),$$

subject to $x_i \in [-5.12, 5.12]$. The global minimum is located at $x^* = (0, \dots, 0)$, $f(x^*) = 0$.

- Styblinski–Tang function: A function with three local solutions and one globally optimal solution in the two-dimensional case:

$$f(x) = \frac{1}{2} \sum_{i=1}^D (x_i^4 - 16x_i^2 + 5x_i),$$

subject to $x_i \in [-5, 5]$. The global minimum is located at

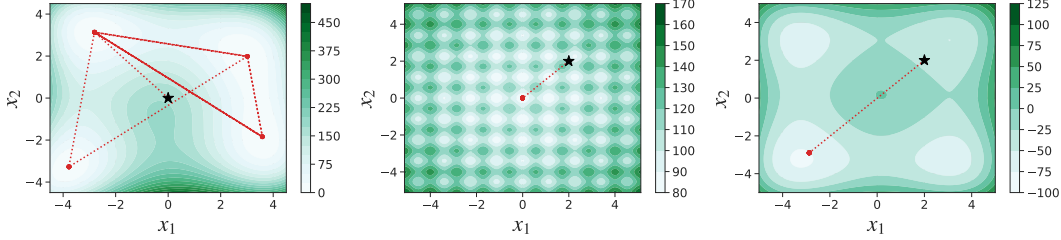
$$x^* = (-2.90353 \dots, \dots, -2.90353 \dots), \quad f(x^*) = -39.16616 \dots \times D.$$

Table 5 shows that the RMSE between the objective function estimated by an MCMC method and the true optimal value:

$$\text{RMSE}_{\text{opt}} = \sqrt{(\bar{f}(x) - f(x^*))^2}, \quad (15)$$

Table 5: Results for each optimization problem. RMSE of the Cost function represents the RMSE between the average cost function estimated by 50,000 MCMC for 10 chains and the true optimal solution.

Target	RMSE _{opt} in Eq. (15)	Annealing steps K	Initial beta β_0	Final beta β_K
Himmelblau (2D)	$1.18 \times 10^{-3} \pm 4.00 \times 10^{-4}$	10	0.1	50
Rastrigin (2D)	$3.00 \times 10^{-5} \pm 1.91 \times 10^{-7}$	10	0.1	50
Rastrigin (10D)	$9.74 \times 10^{-2} \pm 3.22 \times 10^{-4}$	16	0.1	50
Styblinski–Tang (2D)	$1.52 \times 10^{-3} \pm 2.92 \times 10^{-6}$	8	0.1	50
Styblinski–Tang (10D)	$3.58 \times 10^{-3} \pm 9.66 \times 10^{-4}$	15	0.1	50


 Figure 12: Snapshot of the global optimal solution search with AA-VAE-SLMC at $\beta_K = 50$. The red dotted line represents the first 30 transitions. The star point is the initial value. The horizontal and vertical axis indicates the value of each dimension. The contour lines of the left, middle, and right figure represent Himmelblau (2D), Rastrigin (2D), and Styblinski-Tang (2D), respectively.

where $\bar{f}(x)$ denotes the average cost function estimated by 50,000 Monte Carlo steps, under the number of annealing steps K , an initial beta β_0 , and a final beta β_K . The smaller the RMSE_{opt}, the closer the generated samples are to the global optimal, meaning that the optimization problem is solved more accurately. As can be seen from the table, the RMSE is very small in all situations, indicating that the AA-VAE-SLMC can solve the optimization problems even for problems with multiple local optimal and somewhat high dimensionality. Figure 12 shows that snapshots of the transitions of AA-VAE-SLMC for each problem. For the problems with multiple global optimal solutions, the samples should be generated from the global optimal with almost equal probability. In the case of a single global optimal, it is also desirable that the samples be generated in the vicinity of a single global optimal solution, skipping over the local optimal. As can be seen from the figure, for the Himmelblau function with four globally optimal solutions, the samples are generated on the four global optimal with almost equal probability. For the Rastrigin and Styblinski–Tang functions, the samples are generated immediately in the vicinity of the global optimal from the initial state. These global transitions are achieved by the information-rich latent space of well-trained VAE. Such a global transition is not feasible for simulated annealing using the local update and may be an efficient optimization method.

D.6 More Consideration for the Ablation Study in Sec. 4.1

First, we consider the effect of the parallel annealing exchange method by comparing *-VAE-SLMC and *-VAE-ESLMC. From the results of AA-VAE-SLMC and AA-VAE-ESLMC in the bottom figure of Fig. 6, AA-VAE-ESLMC takes a β sequence of a larger interval and reaches $\beta = 1$ earlier than AA-VAE-SLMC although the lower bounds of the acceptance rate AR_{\min} for both methods are same. This result shows the fact that the exchange process between the chains in AA-VAE-ESLMC allows training data with smaller autocorrelation, resulting in more effective model training. For CA-VAE-SLMC and CA-VAE-ESLMC, it is also predicted that the inter-chain exchange process for CA-VAE-ESLMC results in a larger acceptance rate for CA-VAE-ESLMC. More typically, CA-VAE-ESLMC rarely exhibits the same unstable behavior described in Sec. D.1, suggesting that inter-chain exchange increases stability.

Next, we consider the effect of the adaptive annealing method by comparing CA-VAE-* and AA-VAE-*. As can be seen from the figure, the total number of annealing processes can be dramatically reduced by the adaptive annealing method. This result is a significant improvement in efficiency since the computational time for training the model and acquiring the training data during annealing is dramatically reduced, even if the computational time for adaptively determining the beta

in adaptive annealing is taken into account. Retraining after adaptive annealing can also increase the acceptance rate for higher acceptance rates.

Furthermore, we show that the computation time can be reduced due to the pre-training effect. We can confirm the pre-training effect for the reasons that increase of acceptance rates on CA-VAE-SLMC and CA-VAE-ESLMC and interval of beta on AA-VAE-SLMC and AA-VAE-ESLMC as annealing proceeds. These effects are typical behaviors seen in problems other than Gaussian Mixture, suggesting that effects such as pre-training described in the main text Sec. 3.2 are emerging. If the pre-training is observed, the learning results remain almost the same even if much learning is performed in the latter half of annealing, which leads to a significant reduction of training cost of the model as annealing proceeds. In addition, Adaptive annealing of Algorithm 3 can detect insufficient learning, so there is no problem in principle, even if the number of training is reduced. Therefore, scheduling the number of learning times for annealing can be effective. However, comprehensive numerical experiments on scheduling the number of training according to annealing is a future work.

E EXPERIMENT DETAILS

E.1 Model Details

The followings are additional details of the models used in the experiments of the main paper.

Gaussian Mixture. In Sec. 4.1 of the main text, we first define $i_D = (i, \dots, i) \in \mathbb{R}^D$, $\sigma^2 = 0.5\sqrt{D/100}$ and consider the following Gaussian mixture models:

- 2-cluster gaussian mixture:

$$p(x) = \frac{1}{2}\mathcal{N}(-1_D, \sigma^2 I_D) + \frac{1}{2}\mathcal{N}(1_D, \sigma^2 I_D)$$

- 3-cluster Gaussian mixture:

$$p(x) = \frac{1}{3}\mathcal{N}(-1_D, \sigma^2 I_D) + \frac{1}{3}\mathcal{N}(0_D, \sigma^2 I_D) + \frac{1}{3}\mathcal{N}(1_D, \sigma^2 I_D)$$

- 4-cluster Gaussian mixture:

$$p(x) = \frac{1}{4}\mathcal{N}(-3_D, \sigma^2 I_D) + \frac{1}{4}\mathcal{N}(-1_D, \sigma^2 I_D) + \frac{1}{4}\mathcal{N}(1_D, \sigma^2 I_D) + \frac{1}{4}\mathcal{N}(3_D, \sigma^2 I_D)$$

- 5-cluster Gaussian mixture:

$$p(x) = \frac{1}{5}\mathcal{N}(-4_D, \sigma^2 I_D) + \frac{1}{5}\mathcal{N}(-2_D, \sigma^2 I_D) + \frac{1}{5}\mathcal{N}(0_D, \sigma^2 I_D) + \frac{1}{5}\mathcal{N}(2_D, \sigma^2 I_D) + \frac{1}{5}\mathcal{N}(4_D, \sigma^2 I_D)$$

Spectral Analysis. In Sec. 4.2 of the main text, we obtain the data $\{y(kT)\}_{k=0}^{K-1}$ by discretizing $y(\tau)$ with a period T :

$$y(kT) = A_0 + \sum_{i=1}^N A_i \cos(2\pi f_i kT + \phi_i) + r(kT),$$

where $r(kT) \sim \mathcal{N}(0, \sigma^2)$, and we define the following posterior to estimate frequencies f :

$$p(f) \propto \exp\left(\frac{1}{2\sigma^2} \left(y(kT) - A_0 - \sum_{i=1}^N A_i \cos(2\pi f_i T k + \phi_i)\right)^2\right) \mathbf{1}[f],$$

where $\mathbf{1}[f]$ denotes a indicator function such that $\mathbf{1}[f] = 1$ if $f \in [0, 0.5]^N$ and $\mathbf{1}[f] = 0$ if $f \notin [0, 0.5]^N$, which is based on the periodicity outside of $[0, 0.5]^N$. Furthermore, for the sake of simplicity, let assume that T and σ are known, we set $A_0 = 0$, $A_i = 1, \forall i = 1, \dots, N$, $f = (0.1, 0.4, \dots, 0.1, 0.4) \in \mathbb{R}^8$.

Table 6: The annealing conditions for each experiment. The abbreviations and algorithms for each “Method” are summarized in Table.3.

Experiment	Method	β_0	AR _{min}	AR _{max}	ε	T_{check}	Epoch	$n(\mathcal{D}_k)$
Gaussian Mixture	CA-VAE-SLMC	0.1				2,000	150	15,000
	AA-VAE-SLMC	0.1	0.2	1.0	0.01	2,000	150	15,000
	CA-VAE-ESLMC	0.1				2,000	150	15,000
	AA-VAE-ESLMC	0.1	0.2	1.0	0.01	2,000	150	15,000
Spectral Analysis	AA-VAE-SLMC	0.1	0.2	1.0	0.01	2,000	150	15,000
Sensor Problems	AA-VAE-SLMC	0.05	0.2	1.0	0.01	2,000	150	15,000
Optimization Problems	AA-VAE-SLMC	0.1	0.2	1.0	0.01	2,000	150	15,000

Table 7: The training hyper parameters on each experiment for all $k = 1, \dots, K$ in Algorithms 2, 3, and 5.

Experiment	Learning rate	Batch size	β_{VAE}	Input dimension D	Latent dimension M
Gaussian Mixture	1.0×10^{-3}	516	1/120	[2, 10, 25, 50, 100]	[2, 10, 25, 50, 100]
ILG	1.0×10^{-3}	516	6	100	100
SG	1.0×10^{-3}	516	6	2	2
BANANA	1.0×10^{-3}	516	1/20	2	2
RW	1.0×10^{-3}	516	1/20	2	2
Himmelblau	1.0×10^{-3}	516	1/200	2	2
rastrigin	1.0×10^{-3}	1024	1/300	10	10
rastrigin	1.0×10^{-3}	1024	1/300	2	2
Styblinski tank	1.0×10^{-3}	516	1/30	10	10
Styblinski tank	1.0×10^{-3}	516	1/200	2	2
Sensor problem	1.0×10^{-3}	516	1/600	16	16
Spectral Analysis	1.0×10^{-3}	516	1/1000	8	8

E.2 Experimental Conditions for the Annealing VAE-SLMC Methods

We describe the specific hyperparameters of the annealing process of CA-VAE-SLMC, AA-VAE-SLMC, CA-VAE-ESLMC, and AA-VAE-ESLMC for each experiment in Table 6. The algorithms for each method explained in Table 3 are invoked with these hyperparameters. In all the numerical experiments, retrain step in VAE-SLMC (Algorithm 1) and VAE-ESLMC (Algorithm 6) was not performed for each annealing (i.e., $T_{\text{train}} = \infty, \forall k = 1, \dots, K$). We did not perform parallel search in Algorithm 4 for simplicity (i.e., $S = 1$), and sequential search was performed from $\beta'_s = 1$ to input β . T_{max} was set to the value obtained by dividing the interval between $\beta'_s = 1$ and input β by ε .

E.3 Conditions for Training the VAE in VAE-SLMC

In this section, we summarize the parameter settings for model assignment and learning for VAE.

VAE configurations. We define $\text{FC}(i, o, f)$ as a fully-connected layer with input dimension i , output dimension o , and activate function f , and D and M as a input dimension and a latent dimension, respectively. We used the same network and set $M = D$ for all numerical experiments in Sec. 4 and Sec. D. The encoder is composed of $\text{FC}(D, 256, \text{gelu})$ - $\text{FC}(256, 256, \text{gelu})$ - $\text{FC}(256, 128, \text{gelu})$ - $\text{FC}(128, 128, \text{gelu})$ - $\text{FC}(128, 64, \text{gelu})$ - $\text{FC}(64, 32, \text{gelu})$ - $\text{FC}(32, M, \text{gelu})$ and the decoder is $\text{FC}(M, 32, \text{gelu})$ - $\text{FC}(32, 64, \text{gelu})$ - $\text{FC}(64, 128, \text{gelu})$ - $\text{FC}(128, 128, \text{gelu})$ - $\text{FC}(128, 256, \text{gelu})$ - $\text{FC}(256, 256, \text{gelu})$ - $\text{FC}(256, D, \text{gelu})$.

Training hyperparameters. Table 7 summarizes the training parameters other than the network. In all numerical experiments, we use an Adam optimizer and the sum of squared errors (SSE) for the objective function.

E.4 Details of the Replica Exchange Monte Carlo (EMC) and Metropolis–Hastings (MH) Methods in Table 1.

In this section, we show each method and its parameters used in the experiments. For the Metropolis–Hastings (MH) method, we used the proposal with Gaussian distribution $q(x' | x^{(t)}) = \mathcal{N}(x' | x^{(t)}, \sigma^2 I)$ and adjusted the scale parameter σ^2 so that the acceptance rate is between 0.15 and 0.25. In the replica exchange Monte Carlo (EMC) method, the interval of the inverse temperatures is set so that the exchange acceptance rate between replicas is about 0.3 with equal probability by following Nagata and Watanabe (2008). When the kernel of each replica is $q(x' | x^{(t)}) = \mathcal{N}(x' | x^{(t)}, \sigma^2 I)$, we adjusted scale parameter σ^2 so that the acceptance rate is between 0.15 and 0.25. When the kernel of each replica is Hamilton Monte Carlo (HMC) kernel, the number of steps is fixed to 5, and the step size is set so that the acceptance rate is about between 0.4 and 0.6. The EMC method with HMC was implemented using the TensorFlow Probability’s `tfp.mcmc.ReplicaExchangeMC`¹ implementation.

E.5 Detail of Metrics

This section provides the details and purposes of the three metrics used in our experiments.

Root-mean-square error (RMSE). RMSE is defined as the Euclidean distance between the true expected value and its estimate:

$$\text{RMSE}_t = \sqrt{\frac{1}{D} \sum_{d=1}^D (\bar{x}_d^{(t)} - x_d^*)^2}, \tag{16}$$

where $\bar{x}_d^{(t)} = \sum_{t=1}^t x_d^{(t)} / \sum_{t=1}^t 1$ denotes the sampling average of the d -th dimension of the variable at Monte Carlo step t , and x_d^* is the mean of the d -th dimension of the variable mathematically derived from the target distribution. A rapid decrease of RMSE_t means a faster convergence to a mean of the target probability distribution. When all modes of the target distribution cannot be accurately explored, RMSE does not converge to zero.

RMSE is helpful to evaluate whether the samples are biased or not. Furthermore, the convergence rate takes longer if the samples cannot efficiently move between modes. Therefore, we used RMSE in Gaussian mixture experiments in main text Sec. 4.1 to ensure that annealing VAE-SLMC efficiently moves between modes and generates unbiased samples.

Relative error (REM). A summary of the error in approximating the expected value of a variable across all dimensions computed by

$$\text{REM}_t = \frac{\sum_{d=1}^D |\bar{x}_d^{(t)} - x_d^*|}{\sum_{d=1}^D |x_d^*|}, \tag{17}$$

where $\bar{x}_d^{(t)}$ and x_d^* are the same as in RMSE above. REM is divided by the true mean x_d^* to eliminate dependence on the scale for each dimension d . A rapid decrease of REM_t means a faster convergence to a mean of the target probability distribution.

REM is also helpful to evaluate the bias of samples like RMSE. Since REM is scale-invariant by considering the normalization for each dimensional component of sample space, we used REM for the spectral problem in main text Sec. 4.2 and sensor problems in Sec. D.4 where the scales of each dimension are different.

Effective sample size (ESS). ESS is a common measure to evaluate efficiency of sampling algorithms. The ESS represents the estimated number of iid samples generated. When measuring ESS in higher dimensions, it is common to consider ESS for each dimension. For a sequence of samples $(x^{(t)})_{t=0}^T$, the effective sample size (ESS) was computed as

$$\text{ESS} = \frac{1}{1 + 2 \sum_{t=1}^{\hat{T}} \hat{\rho}_t}, \tag{18}$$

where \hat{T} is the stopping time. $\hat{\rho}_t$ is an estimate of the lag- t autocorrelations of the Markov chain:

$$\hat{\rho}_t = \frac{1}{N-t} \sum_{r=1}^{N-t} (x^{(r)} - \bar{x})(x^{(r+t)} - \bar{x}). \tag{19}$$

¹https://www.tensorflow.org/probability/api_docs/python/tfp/mcmc/ReplicaExchangeMC

The ESS is calculated by using TensorFlow Probability's `tfp.mcmc.effective_sample_size`² implementation. If an MCMC simulation generates completely independent samples, then $ESS = 1$. We report the mean across 10 runs of minimum ESS across dimensions and the 1st and the 2nd moments.

ESS is a helpful measure to quantify the correlation between samples and to see the number of samples that are effectively independent and is the most commonly used evaluation measure in Bayesian estimation for gradient-based MCMCs such as HMC. On the other hand, it is difficult for ESS to capture whether the transition between modes is efficient visually. Therefore, in the performance evaluation of Naïve VAE-SLMC in Sec. D.2, we use ESS as the metric because it is not a particularly multimodal distribution, and we wanted to confirm its superiority over HMC for distribution families that HMC is not good at.

²https://www.tensorflow.org/probability/api_docs/python/tfp/mcmc/effective_sample_size